Article:
Bourgeois, E, Bouniol, D, Couvreux, F et al. (2018) Characteristics of mid-level clouds over West Africa. Quarterly Journal of the Royal Meteorological Society, 144 (711). pp. 426-442. ISSN: 0035-9009

https://doi.org/10.1002/qj.3215

Characteristics of mid-level clouds over West Africa

Elsa Bourgeois [a *], Dominique Bouniol [a], Fleur Couvreux [a], Françoise Guichard [a],

John Marsham [b,c], Luis Garcia-Carreras [b], Cathryn Birch [b], Doug Parker [b]

[a] CNRM, CNRS/Météo-France, Toulouse France

[b] Institute for Climate and Atmospheric Science, School of Earth and Environment, University of Leeds United Kingdom

[c] National Centre for Atmospheric Science, School of Earth and Environment, University of Leeds United Kingdom

* Correspondence to: E. Bourgeois, Météo France, GMME,

42 avenue Gaspard Coriolis, Toulouse 31057, France.

E-mail: elsa.e.bourgeois@gmail.com

Abstract

Mid-level clouds, located between 2 and 9 km height, are ubiquitous in the tropical belt. However, few studies have documented their characteristics and tried to identify the associated thermodynamical properties, in particular in West Africa. This region is characterized by a strong seasonality with precipitation occurring in the Sahel from June to September (monsoon season). This period also coincides with the annual maximum of the cloud cover. Here, we document the macro- and microphysical properties of mid-level clouds, the environment in which such clouds occur, as well as their radiative properties across West Africa. To do so, we combined high resolution observations from two ground-based sites (including lidar and cloud radar) in contrasted environments: one in the Sahel (Niamey, AMMA campaign, 2006) and the other in the Sahara

This article has been accepted for publication and undergone full peer review but has not been through the copyediting, typesetting, pagination and proofreading process, which may lead to differences between this version and the Version of Record. Please cite this article as doi: 10.1002/qj.3215

(Bordj Badji Mokhtar, Fennec campaign, June 2011) along with the merged CloudSat-CALIPSO satellite products. The results show that, mid-level clouds are found throughout the year with a predominance around the monsoon season early in the morning. They also are preferentially observed in the southern and western part of West Africa. They are usually thin (most of them are less than 1000 m deep) and as observed in Niamey, mainly composed of liquid water. A clustering method applied to Niamey data allows to distinguish three different types of clouds: one with low bases, one with high bases and another with large thicknesses. The two first cloud families are capped by an inversion. The last family is associated with a large vertical moisture transport and likely has the highest radiative effect at the Earth's surface among the three cloud types.

Key Words: mid-level clouds; diurnal cycle; macrophysical and microphysical properties; thermodynamics; radiative impacts; ground-based and spaceborne observations; West Africa

1. Introduction

Clouds have a major impact on the distribution of water and energy fluxes within the atmosphere (Zhang and Rossow, 1997; Weaver, 2003; Kato *et al.*, 2008; Stephens, 2005). Clouds also represent one of the main sources of uncertainties in global climate models as a result of the difficulty of parametrizing cloud-related processes and their interactions. This paper focuses on mid-level clouds often considered as clouds with a base lying above 2 km, while their tops can reach up to 9 km (e.g. Sassen and Wang, 2012).

Historically, clouds have largely been documented by ground-based observers and later by remote sensing instruments either located at the ground or on-board satellites. Mid-level clouds are difficult to sample with geostationary satellites, especially when they are part of a multi-layer cloud scene, together with low clouds (e.g., cumulus) or high clouds (e.g., cirrus) (Tompkins and Adebiyi, 2012). This is why profiling instruments are essential to document clouds in the mid-troposphere.

The launch of CloudSat (Stephens *et al.*, 2002) and *Cloud-Aerosol Lidar and Infrared Pathfinder Satellite Observations* (CALIPSO) (Winker *et al.*, 2007) provided a vertically resolved view of clouds at the global scale (Sassen and Wang, 2008). By examining a global CloudSat derived cloud climatology, Riley and Mapes (2009) found two distinct peaks of cloud occurrence at mid levels in the Tropics: the first in the vicinity of the melting zone at 0°C, located at about 5 km height, where the mid-level cloud frequency of occurrence is generally maximum, and the second at about 7-8 km height, towards -15°C. Haynes and Stephens (2007), Wang *et al.* (2000) and Riihimaki *et al.* (2012) also observed this bimodal structure. Sassen and Wang (2012), using CloudSat and CALIPSO data, documented the climatology of mid-level clouds in the tropical belt. They highlighted a large amount of altocumulus that occurred in conjunction with deep convection during monsoon season. During this period, mid-level clouds are mainly found over land: in the north of South America, West and Central Africa, north of Australia but also over sea, in particular in the Tropical Pacific Ocean. Other documentations of mid-level clouds come from ground-based measurements either obtained during field campaigns or through systematic observations as performed at the ARM (Atmospheric Radiation Measurement) sites (Bouniol et *al.*, 2012; Mace et *al.*, 2006; Riihimaki et *al.*, 2012).

Johnson *et al.* (1999) have shown that the distribution of cloud tops is trimodal with the *Tropical Ocean and Global Atmosphere Coupled Ocean-Atmosphere Response Experiment* (TOGA COARE; Webster and Lukas, 1992) data: it includes shallow cumulus at the stable trade wind layer (cloud tops around 2 km), cumulus congestus (cloud tops around 5 km) and deep cumulonimbus extending up to the tropopause (cloud tops around 15-16 km). The occurrence of mid-level clouds is then related to an enhanced stability layer at the 0°C level. Riihimaki *et al.* (2012) made use of 4-yr of vertically pointing lidar and radar measurements deployed at the ARM site at Darwin (Australia) to produce a climatology of mid-level clouds. These observations emphasize the occurrence of many thin clouds (70% being less than 2 km thick) with cloud top heights between 4 and 9 km. These mid-level clouds have a strong diurnal cycle, with a maximum frequency of occurrence at

night and in the morning and a minimum around noon. As Johnson *et al.* (1999), Riihimaki *et al.* (2012) explain the development of mid-level clouds at Darwin by detrainment from congestus and cumulonimbus especially in break monsoon periods. For the active monsoon periods, mid-level clouds would be formed by melting-cooling mechanism (Johnson *et al.*, 1996; Yasunaga *et al.*, 2006). The melting-cooling mechanism is explained by stratiform precipitation which are predominantly composed of ice and generates through the melting process an atmospheric cooling. The existence of such a colder zone is thus more favorable to the condensation and further helps the formation of thin mid-level clouds.

Few studies have documented the mid-level clouds in West Africa. Using brightness temperatures obtained from Meteosat for three consecutive summers (June to September, 1983 to 1985), Duvel (1989) built a climatology of cloudiness over this region, and highlighted the occurrence of clouds, with cloud tops around 500 mb, with a preferred occurrence at sunrise and a lower occurrence at noon. Twenty years later, Stein *et al.* (2011) used CloudSat-CALIPSO data to show the expansion of a cloud layer between 600 (~ 4200 m) and 400 (~ 7200 m) hPa across West Africa during the monsoon period. They also showed how over the Sahel these clouds are at the top of the Saharan Air Layer (SAL, which corresponds to dry and hot air with high dust loadings) (as noted by Parker *et al.*, 2005) and extend over the Sahara where they are at the top of the Saharan Convective Boundary Layer, or Saharan Residual Layer (SRL) (Marsham *et al.*, 2013; Garcia-Carreras *et al.*, 2015). Their cloud top temperatures are generally below freezing, but they do not necessarily include ice (Ansmann *et al.*, 2008). These Saharan clouds may be a key ingredient in the radiative budget of the Saharan Heat Low (SHL) (Marsham *et al.*, 2016). In the Sahel, Bouniol *et al.* (2012) analysed the observations at the ARM Mobile Facility (AMF) installed in 2006 at Niamey (Niger) for the African Monsoon Multidisciplinary Analysis (AMMA) field campaign (Redelsperger *et al.*, 2006). As during TOGA-COARE, they found between April and September, three peaks in the vertical profiles of cloud occurrence associated with low-level clouds, mid-level clouds and cirrus superimposed to deep convective cloud occurrence. They further highlighted the

large radiative impact of mid-level clouds at the surface both in the shortwave and in the longwave domains.

Mid-level clouds represent a real challenge for global climate models. Indeed, those models very often underestimate mid-level cloud frequency (Zhang *et al.*, 2005) and their radiative effects. Moreover, in a process-oriented evaluation of climate models from the *Cloud Feedback Model Intercomparison Project* component of CMIP5 in the northern Africa [10°W-10°E, 5°S-45°N], Roehrig *et al.* (2013) also showed that climate models underestimate the mid-level cloud fraction. In addition, Tan *et al.* (2016) show that the underestimation of the supercooled liquid fraction may lead to a severe underestimation of the equilibrium climate sensitivity. The mixed-phase processes are a major challenge for constraining climate models. In order to improve the representation of mid-level clouds within models, we need to document them further, and to better understand their origins, properties and impacts.

This motivates the present study, which aims to document the properties of these clouds, the environment in which they occur, as well as their radiative effect across West Africa. The novelty of this study lies in the joint analysis of several unique (and independent) observational data sets of mid-level clouds over West Africa. Section 2 describes the data used in this study to document these clouds: two ground-based observational datasets and one satellite product. Section 3 presents the methodology used to detect the mid-level clouds and the clustering methods used to identify different types of mid-level clouds. Methods used to analyse the thermodynamic profiles and the radiative impacts of these clouds are also described in this section. The regional climatology of these clouds obtained with CloudSat-CALIPSO data is developed in section 4. In this same section, the characteristics of mid-level clouds obtained for ground-based sites are presented. We also discuss the processes associated with these mid-level clouds as well as their radiative properties. Concluding remarks and perspectives are finally given in section 5.

2. Data

2.1. Cloud vertical profiles derived from ground-based sites

Observations from two ground-based sites have been used in this study (see Table 1 for details on measured and computed parameters and spatial and temporal sampling). The first site is located in Niamey (13.58°N, 2.38°E, ~200 m above mean sea level, Niger (see Fig. 1a)), where the ARM Mobile Facility (AMF) was deployed for one year in 2006 (Miller and Slingo, 2007). It gives high-frequency information about cloud macrophysical and microphysical characteristics, precipitation, surface radiative fluxes, and aerosols (Stokes and Schwartz, 1994). This facility includes in particular a Doppler radar operational from April 2006, a Micropulse Lidar and radiosondes (with an increase in their frequency to 3 hours for two special observing periods in June and August). Pyranometers and pyrgeometers are also used to measure the radiative fluxes. Other instruments provide near-surface meteorology.

The second ground-based site used in this study is located at Bordj Badji Mokhtar airport (BBM, 21.38°N, 0.92°E, ~420 m above mean sea level, Algeria (see Fig. 1a)) in the Sahara. It was instrumented for the Fennec campaign in June 2011 (Marsham *et al.*, 2013) with several instruments among which was a Doppler lidar.

At the Niamey site, cloud identification from the vertically pointing radar and lidar measurements has been performed with the standard Cloudnet target categorization algorithm (Hogan and O'Connor, 2004; Illingworth *et al.*, 2007). The output of this algorithm is a cloud mask with a temporal resolution of 43 seconds and a vertical resolution of 60 meters. Each cloudy pixel is also characterized in term of phase thanks to the combination of the various radar/lidar measurements. When only the lidar was available, at BBM and between the 1st January to the 31st March 2006 at Niamey (see Table 1), a cloud mask has been built directly from the lidar measurements. In this case, no insights on the cloud phase or microphysical properties are available.

2.2. Spaceborne observations from CloudSat-CALIPSO

CloudSat-CALIPSO cloud samplings are also used to build a regional climatology of the occurrence of mid-level clouds in West Africa (see Table 1). Both CloudSat (Stephens *et al.*, 2002) and CALIPSO (Winker *et al.*, 2007) belong to the A-Train satellite constellation and cross the equator at 0130 (night) and 1330 (day) local time (LT) (but all time in the paper are in UTC). The constellation has the same ground track every 16 days. They provide data from a spaceborne Cloud Profiling Radar (CPR) (94 GHz nadir-looking radar with a sensitivity of -31 dBZ (Haynes and Stephens 2007; Stephens *et al.*, 2008) and a profiling cloud lidar (CALIOP). Both measurements are combined in the CloudSat 2B-CLDCLASS-LIDAR on the CloudSat grid providing spatial/height cross-section (1.5 km across-track by 2.5 km along-track radar footprint and 240 m vertically) with 0.16 seconds temporal resolution. This product already provides a cloud classification (see Sassen and Wang, 2008). As a wish of homogeneity among the different datasets, this classification was not used and the same basic cloud classification principle, used at Niamey, has been applied to the CloudSat-CALIPSO combination across West Africa. Those products have been extracted from 0-45°N and -20°W-50°E and limited from June 2006 to May 2010 (four full years) because since January 2011 only daytime measurements are available for the CloudSat radar.

3. Methods

3.1 Cloud object identification

Different cloud types (shallow convection, mid-level clouds, convection and cirrus) are identified using the basic morphological criteria proposed by Bouniol *et al.* (2012) with a temporal resolution of 30 minutes and a vertical resolution of 100 m below 5 km, 200 m between 5 and 10 km, and 400 m above (built from the native 30-second and 42-meter resolution). First, each cloudy

column is examined. Then, a pixel is considered cloudy if the cloud fraction is at least 2% (same method carried out in Bouniol *et al.* (2012) for the detection of clouds). Each cloud having a base higher than 3 km and/or a top lower than 8 km (9 km at BBM) is labelled as a mid-level cloud. For Niamey, the cloud base must also be located at least 1 km above the LCL in order to not include boundary-layer clouds as mid-level clouds. At BBM, 22 cloud objects identified below 3.8 km were discarded because of their too small attenuating backscattering coefficients. Then a region-growing technique using a four connectivity criterion is applied on the time series in order to group together contiguous profiles containing mid-level clouds and contiguous cloud sheets that do not exactly match the altitude criteria (i.e. two pixels belong to the same cloud if they have one edge in common). A labelling process is also applied in order to identify each individual cloud as a cloud object. In general and as found by Riihimaki *et al.* (2012), mid-level clouds are composed of liquid droplets, ice, melting ice or supercooled liquid droplets. In the identification process, rain and drizzle pixels are not considered as clouds. At BBM, the brightness temperature of mid-level clouds obtained from Meteosat, typically from 260 to 270 K, was used to confirm the presence of mid-level clouds when the lidar was non-operational for a short period (no longer than 3 hours). This method is similar to Bühl *et al.* (2016). Note that the instruments do not have the same sensitivity, this will thus affect the comparison of cloud property to some extent.

3.2. Cloud characteristics

For both ground-based and spaceborne samplings, the same process is applied to identify mid-level clouds. An illustration of the identification process is shown for the 21 July 2006 in Figure 1. The left panel shows the temporal evolution of vertical profiles of radar reflectivity (b) and lidar backscattering (c) at Niamey and in the right panel for the CloudSat-CALIPSO transect beginning at 1247 UTC (UTC = LT - 1 at Niamey and BBM sites), the latitude-altitude of radar reflectivity (d) and the cloud fraction deduced from the lidar signal in the CloudSat grid (e) between

3°N and 31°N. At Niamey, three identified mid-level clouds are contoured in cyan. For each detected mid-level cloud in ground-based and spaceborne observations, cloud base height (B), cloud top height (T), cloud thickness by cloudy column (i.e. the variables of each cloudy column detected for all cloudy objects have been recovered) and by cloud object (i.e. the variables of each cloudy column pertaining to a single cloudy object have been recovered and averaged to have a mean value for this cloud) as well as the starting time, ending time and therefore a ‘’duration’’ have been stored. This "duration" corresponds to the time spent above the ground instruments. Note that the lidar signal may be extinguished by a strong concentration of particles in the lower layers (i.e. optically thick aerosols and/or clouds and/or precipitation). Therefore, when the lidar is the only instrument, cloud top height may not be accurately detected; consequently at BBM and between the 1st January to the 31st March 2006 at Niamey in particular, there are more uncertainties in cloud top height and cloud thickness estimates. However, the lidar is the only instrument able to detect optically thin clouds (as shown in Ansmann *et al.*, 2009), therefore even when the radar was operating, some clouds are detected by the lidar only. Moreover, in some situations cloud radars can suffer from strong attenuation and therefore cloud top height may not be accurately detected. This is for instance the case when precipitation are present. Consequently, instrumental effects can lead to some bias in the cloud top statistics. At Niamey, the Doppler capability of the radar, the polarization of the lidar and the post-processing through the categorization algorithm allow us to identify precipitation below cloud and the fraction of hydrometeor types within the cloud (i.e., cloud liquid droplets, ice, melting ice or supercooled liquid droplets). The radar measurements also provide the reflectivity which may be used as a proxy for the microphysical properties, the Doppler velocity and the spectral width. The CloudSat radar only measures reflectivity and more generally for the spaceborne devices, the cloud top height may be accurately detected while along-path attenuation (on both lidar and radar) can lead to a non-detection of the cloud base height.

3.3. Clustering methods

A visual inspection of the time series or of the spaceborne samples over West Africa shows a wide diversity in mid-level cloud macrophysical and microphysical properties. In order to group mid-level clouds into categories sharing similar characteristics, a cluster analysis has been applied. Clustering techniques are commonly used in meteorological applications. Recently cluster analysis has been used to separate cloud families with ground-based and spaceborne lidars for cirrus (Hoareau *et al.*, 2013), and with geostationary satellite data for tropical mesoscale convective systems (Pope *et al.*, 2009a). Jakob and Tselioudis (2003) also used a clustering method to analyse ISCCP cloud products in the tropical western Pacific region.

Some caution is required with clustering methods as, by design, they always provide a result. Therefore, in order to gain confidence in the analyses, two fundamentally different cluster algorithms, the K-means method (MacQueen, 1967) and the Hierarchical Agglomerative Clustering (HAC) algorithm (Jain and Dubes, 1988), have been systematically applied, and the results obtained with each of the two methods have been compared. K-Means clustering is a partitioning method that allows to optimally split the set of objects in a fixed pre-determined number of K groups. The HAC algorithm is based on the computation of Euclidean distance following the "Ward criterion" (Ward, 1963), whose aim is to have a minimum gain of intra-group inertia at each aggregation. It produces a sequence of nested groups into each other that can be visualized with a dendrogram allowing the identification of the optimum number of clusters.

In order to select the variables for the clustering analysis, a Principal Component Analysis (PCA) was applied on cloud variables observed at Niamey site. Cloud base height and cloud thickness explain the largest part of the variances among the different clouds. In addition, those two variables are available at both Niamey and BBM sites and can be retrieved in satellite data. In this study the clustering methods are applied to Niamey data. In future work, they will be applied to the other data.

3.4. Thermodynamic profiles

In order to analyse whether mid-level clouds are associated with a particular thermodynamic stratification and if these mid-level clouds induce changes in these profiles, the radiosondes launched between two hours before the starting time of a cloud occurrence and the starting time of a cloud occurrence are referred to as “before” in the following and the radiosondes launched between the ending time of a cloud occurrence and two hours after the ending time of a cloud occurrence are referred to as “after” in the following. The radiosondes launched when a mid-level cloud is present are referred to as "during". The radiosondes, where a mid-level cloud lasts for more than one hour, are retrieved and composited at Niamey. All radiosondes have been interpolated onto a regular 40 m grid.

Each radiosonde is also examined in order to detect an enhanced gradient of potential temperature referred to here as “inversion” (Haikin et al., 2015). An inversion layer is detected between 100 and 9000 m when:

$$\frac{d\theta}{dz} \geq \overline{\frac{d\theta}{dz}} + 2\,\sigma \qquad (4)$$

$\frac{d\theta}{dz}$ the vertical gradient of the potential temperature (1),

$\overline{\frac{d\theta}{dz}}$ the mean of the vertical gradient of the potential temperature (2),

σ the standard deviation of the mean of the vertical gradient of the potential temperature (3), Once an inversion is detected, its base is determined up to the first point where:

$$\frac{d\theta}{dz} \leq \overline{\frac{d\theta}{dz}} \quad \underline{\text{below}} \text{ the maximum of the inversion (5)}$$

and its top is determined up to the first point where:

$$\frac{d\theta}{dz} \leq \overline{\frac{d\theta}{dz}} \quad \underline{\text{above}} \text{ the maximum of the inversion (6)}$$

The depth of the inversion is then the distance between them the inversion top and the inversion base. Several inversions are generally detected in a given radiosonde, therefore for each mid-level cloud, the nearest inversion was selected.

3.5. Radiative impacts

As the visual examination of the data over West Africa reveals a large variety in the macrophysical properties, different radiative properties may also be expected between the different mid-level cloud types. The radiative impact of clouds at the surface is defined as the difference between the downward flux at the surface and the clear-sky downward flux (Ramanathan *et al.*, 1989).

If full-sky radiative measurements are performed at both ground-based sites, one still needs to estimate the clear-sky shortwave downwelling fluxes. Two methods, by cloudy column, can be implemented as described in Bouniol *et al.* (2012): i/ either by compositing all the observations in clear-sky conditions for a given month, ii/ or by estimating for each day the shortwave downwelling flux in clear-sky thanks to the shortwave fluxes at the top of atmosphere (TOA) calculated from the solar zenith angle, fitted by a coefficient, corresponding to the atmosphere transmissivity, to the shortwave clear-sky observations available during that day (between 0500 UTC to 1900 UTC). This fitting can only be performed if some clear-sky observations exist during that day. For the longwave domain, we have applied the method described in (i) but this method should be taken with caution because it introduces bias as mean conditions with cloud are moister than mean conditions without. Moreover, the day to day variability of the clear-sky downwelling fluxes is not taken into account. The shortwave and longwave fluxes at the TOA obtained from the Geostationary Earth Radiation Budget (GERB) Binned Averaged Rectified and Geolocated (BARG) (Harries *et al.*, 2005) data have been used to determine the TOA_SW_n and the TOA_LW (see Table 2). The measured shortwave and longwave fluxes are retrieved only when mid-level clouds are the only cloud type in

the column. In order to reduce noise either in the measurements or in the clear-sky estimates, observations are sampled over 15 minutes.

4. Results

4.1. Regional climatology of mid-level clouds

From the four-year of CloudSat-CALIPSO, a mid-level cloud climatology has been built across West Africa (3.575-31.575°N; 14.78°W-28.47°E). In each satellite track, mid-level clouds are identified and labelled. West Africa has been divided in elementary box (3.5° lat x 3.09° lon) that contains approximately two daytime and two nighttime transects per day. The number of clouds normalised by the track length in kilometres, referred to as "density", is computed in each box. Oceanic and coastal regions have been discarded except for the Guinea Gulf (see Figure 2).

43115 mid-level clouds were observed in this four-year sample. The map of yearly-mean density of mid-level clouds is presented in Fig. 2a. This figure indicates that clouds occur approximately twice as frequently in the southern part of West Africa than in the North. More clouds are also observed in the western than in the eastern part, and this zonal gradient is even amplified in the Sahara and in the Sahel. The spatial structure of this zonal pattern suggests that it could be influenced by the dynamics of the SHL, since the maximum occurrence of mid-level clouds and the location of the climatological SHL both move accordingly through the season; the SHL being located in the southeastern part of West Africa in winter and in the northwestern part in summer (Lavaysse *et al.*, 2009). This zonal gradient is maximum during the West African monsoon season and vanishes from October to March when the cloud occurrence is much smaller. More broadly, for JAS, Fig. 2d indicates the presence of clouds all over West Africa with strong maxima in the south-eastern and in the Guinea Gulf regions. Another local maximum is observed on the south-eastern flank of the SHL (15-22°N; 6°W-4°E) (see Fig. 4 of Lavaysse *et al.*, 2009), and an

increase of the occurrence of mid-level clouds up to the north of the Sahara Desert. This extent is consistent with the preferential advection of moisture northwards associated with the Hoggar (Cuesta *et al.*, 2010) and cloud downstream (i.e., West) of the convective maximum seen in Fig. 11a of Pantillon *et al.* (2016). At the seasonal scale, mid-level clouds appear to be associated with the northward progression of the monsoon from spring to summer and its withdrawal in fall. This is consistent with both generation through detrainment from deep convection, and moist convection at the top of the Saharan atmospheric boundary layer, which is deepest in summer.

The annual cycle of these clouds is shown in Fig. 2f where the results are presented for latitudinal bands. At all latitudes, there is a marked annual cycle with an increase of mid-level cloud occurrence during the West African monsoon and a decrease between November and February. However, in the northern Sahara, the amplitude of the annual cycle is much lower, and we also observe a slightly different behaviour with a narrower maximum which is shifted later in the season (in August-September as opposed to June-July-August). Tropical plumes (TP), observed at the north of West Africa and mainly in autumn, winter and spring, could also explain the presence of mid-level clouds in these regions since they consist of long lasting, large-scale, partly precipitating mid-level cloud layers (Fröhlich *et al.*, 2013; Knippertz and Fink, 2009). The northern latitudinal bands in Fig. 2f show an indication of TPs with an increase occurrence of these clouds in spring and autumn. North-South differences are therefore observed in relation with the monsoon dynamics and consistent with a role of mid-latitude wintertime systems in the northern Sahara.

The distributions of mid-level cloud bases, tops and thicknesses obtained from CloudSat-CALIPSO data indicate that the mean cloud base lies between 4 and 5 km and the mean top between 5 and 6 km, while cloud thicknesses are less than 3 km with a peak around 300 m. These results are consistent with Bourgeois *et al.* (2016) who also observed mid-level cloud tops between 4.5 and 6.5 km in the tropics using CALIPSO data and found cloud thicknesses around 400 m in average over land.

The CloudSat-CALIPSO data, which cover a period of four years, are well suited to analyse

the annual cycle whilst keeping a homogeneous sampling between day (13:30 LT) and night (01:30 LT). However, this scarce sampling of the diurnal cycle may introduce some biases. This will be addressed below with high-frequency ground-based data obtained at Niamey and BBM.

4.2. Occurrence frequency and diurnal cycle of mid-level clouds

Bouniol *et al.* (2012) described the clouds encountered over Niamey from April to September 2006; however, so far, mid-level clouds and the thermodynamics environment within which they occur have not been extensively studied in this region. In this section, we extend this study to the entire year 2006 for mid-level clouds.

The monthly-mean cloud frequencies of occurrence, defined for a given altitude as the number of cloudy pixels over the total number of pixel observations, depicted in Figure 3 shows that mid-level clouds were observed all year round in 2006 except in December. 482 mid-level clouds are observed with a larger occurrence during the monsoon period (more than half of the clouds are observed in JJAS) in agreement with the satellite data. The monthly-mean diurnal cycle of their occurrence (see Fig. 4) indicates that, for each month, mid-level clouds are present throughout the day with a peak in the early morning, between 0200 UTC and 0600 UTC, during the monsoon period, in agreement with previous studies (Duvel, 1989; Riihimaki *et al.*, 2012). It is interesting to note that in spite of the different diurnal cycle of convective events in the Pacific Ocean and in West Africa, with a later triggering in West Africa (mid to late afternoon) than in the Pacific Ocean (preferential triggering in the morning), the maximum in the diurnal cycle of mid-level clouds occurs in the early morning in both studies. During winter and autumn, the occurrence of mid-level clouds does not show any preferential hour. The same data obtained from the BBM site are also shown in Figures 3 and 4. This site is located further north and is therefore subject to different meteorological conditions when compared to Niamey (Marsham *et al.*, 2013; Gounou *et al.*, 2012; Cuesta *et al.*, 2008). Ninety four mid-level clouds were observed in June 2011, compared to 54 at

Niamey in June 2006 while the cloud climatology at BBM obtained from the CloudSat-CALIPSO data does not show that there are more clouds at BBM than at Niamey (see Fig. 5c). This can be due to the track numbers of CloudSat-CALIPSO which differ from month to month, as well as to the lidar operation, which may oversegment clouds due to interruption in operation. Interannual variability may also explain this difference. The frequency of occurrence of mid-level clouds at BBM is higher than at Niamey, and both peak around 6 km height (see Fig. 3). At BBM, the amplitude of the diurnal cycle is weaker than at Niamey, and the maximum is shifted to between 1600 UTC and 2000 UTC. In Figure 4, white dots at BBM indicate the fraction of time where the lidar was operating. There are more missing data around the maximum of cloud occurrence. At around 1830 UTC, for example, there is almost half of the time a mid-level cloud detected but the lidar operated only 60% of the time at this hour. So this diurnal cycle should be taken with caution.

4.3. Morphology and microphysics of mid-level clouds

Figure 5a shows the cloud base height distribution and the column base height distribution observed at these two locations. At Niamey, for the whole year, cloud bases vary between 2550 m and 7650 m with a peak around 5000 m (and cloud tops between 3000 and 8500 m with a peak around 5500 m (see Fig. 6b)), and a comparable histogram is obtained for June only, with however less high cloud bases. At BBM, cloud bases vary between 4000 m and 8400 m with a peak around 5600 m. The column base height distributions (dashed lines) are close to the cloud base height distributions (solid lines). At Niamey, an increase of cloud bases is observed in JFM, with a peak around 6000 m, followed by a decrease with a minimum of about 4600 m in October and November (not shown). During the monsoon period, the cloud base height remains close to 5100 m. Cloud bases at BBM in June 2011 are slightly higher than at Niamey in June 2006 especially in the morning from 0000 UTC to 0600 UTC (not shown). Sounding data indicate that cloud bases detected at this station are at the same altitude as the top of the SRL in the morning (at 0300 UTC

and 0600 UTC) (not shown); this may explain the high altitudes of the bases at BBM. Note that, at BBM, some cloud bases might be too low because some virgae might be interpreted as cloud instead of precipitation.

Most mid-level clouds have a small vertical extent (Fig. 5b). Indeed at Niamey, 342 mid-level clouds have a thickness smaller than 500 m and 83 between 500 m and 1000 m. So, 88% of clouds have a thickness smaller than 1 km whereas Riihimaki *et al.* (2012), over the Pacific, only found 50% with a similar instrumental design. Very few clouds have a thickness larger than 1000 m, with only 47 between 1000 m and 2000 m and 10 thicker than 2000 m. These thicker clouds mainly occur during the monsoon period. According to Figure 5b, on average, at Niamey the thickness is about 460 m for the entire year of 2006 and 520 m for June 2006. At BBM, a 570 m mean thickness, similar than at Niamey, is found. The thickness derived by cloud objects is lower than the one derived by columns. Nevertheless, both analyses confirm thinner clouds at Niamey than at BBM. The analysis of the variation of thickness throughout the diurnal cycles indicates that the thicknesses at Niamey are however larger than at BBM in the early morning this can be due to the lidar which does not see through thick clouds and misses the deepest clouds (not shown). These first results are consistent with the CloudSat-CALIPSO climatology. Comparisons of cloud frequency of occurrence between ground-based and spaceborne radar-lidar (Bouniol *et al.*, 2012; Protat *et al.*, 2014) show a slight overestimation in the mid-level clouds for the spaceborne dataset. Protat *et al.* (2014) relate this overestimation to the ability of the CALIPSO to detect clouds in the low levels while the ground-based lidar may be extinguished either by low-level liquid clouds or by large amount of aerosols as found in the Niamey region. This point may explain the ability of the CloudSat-CALIPSO combination to detect lower cloud bases as well as thicker clouds.

In the following, the analysis will be made by cloud objects in order to differentiate mid-level cloud families. Histograms of cloud base height, top height, thickness, liquid, ice and mixed phase fractions, reflectivity and standard deviation of reflectivity are shown by the blue curves in Figure 6 for the 482 cloud objects observed at Niamey in 2006.

Reflectivities are between -40 and -5 dBZ with a peak at -32 dBZ and their standard deviations spread from 0 to 27 dBZ with a peak at 3 dBZ (see Fig. 6e-f). Clouds having the higher reflectivities, i.e. greater than -15 dBZ, also have a larger variance. There are few clouds with high water contents even if a second very slight peak of reflectivity is observed at -22 dBZ. In CloudSat observations, the reflectivity, obtained with the files 2B-GEOPROF, shows a peak at -22.5 dBZ with fluctuations between 11.2 and -28.25 dBZ. One should keep in mind that the reflectivity distribution only concerns a sub-sample (62%) of the mid-level clouds observed at Niamey. Indeed in JFM, the radar was not operational (see Table 1), and 72 mid-level clouds were detected by the lidar alone. The thinnest clouds (less than 1000 m depth) are hard to detect with the radar, leading to 212 mid-level clouds that are very partially sampled (with for all these cloud objects less than 25% of the total number of cloudy pixels sampled by the radar) among which 109 are not detected at all by the radar. This means that these geometrically thin clouds are mainly composed of small hydrometeors. Conversely, the thicker clouds are better sampled by the radar (198 are well detected ($\geq$25%)); their thickness can be as large as 4 km. This analysis is valid for all months of 2006 except when no clouds are detected (e.g. December).

At Niamey, the composition of clouds in term of hydrometeors can be documented with the categorization algorithm. The fractions described below concern cloud volume. Mid-level clouds are mainly composed of ice and liquid water with a predominance of liquid water (see. Fig. 6d): 73 % of clouds are composed of at least 50 % of liquid water and 80 % of clouds are composed of at most 20 % of ice. During the monsoon period, 30 % of the clouds also contain supercooled liquid droplets but in small quantities and 16 % contain supercooled liquid droplets at their cloud tops. In the same region, Stein et al. (2011) found that approximately 20% of mid-level clouds contain supercooled liquid water at their cloud tops (their Fig. 6), which is consistent with the present study. Ansmann *et al.* (2009) observed a high frequency of occurrence of mixed-phase clouds compared to other clouds with cloud top temperature around -30°C. At Niamey site, the clouds with more than 75% mixed-phase at their top have their cloud tops located at around 6-7 km (not shown). In

addition, some clouds also contain drizzle or rain associated with liquid water droplets, particularly during the monsoon period. Only between May and September, some clouds are almost exclusively composed of ice, but they are relatively few: one cloud in May and one in August, three clouds in June and in July and four clouds in September.

On the other hand, the clouds observed at Niamey site are mostly non-precipitating and of "short duration" (for 41 % of them, the time during which they are observed above the instruments is lower or equal to 30 minutes, mainly observed during JAS). In JFM, "durations" can be greater than five hours which might be associated with TP events.

Overall, no obvious correlations emerge between the different cloud characteristics; for example both very thick and thin clouds can have high cloud-averaged reflectivity. In order to objectively group together clouds sharing similarities, clustering methods are applied on mid-level cloud base and thickness variables.

For brevity, only results obtained with the HAC algorithm using the "Ward criterion" are shown in this paper as results obtained with the K-Means method were very similar. In Figure 7, the dendrogram clearly isolates three different clusters: one with low bases (in blue, cluster 3), one with high bases (in red, cluster 2) and another with high thicknesses (in green, cluster 1). The associated scatter plot of cloud thickness as a function of cloud base is shown in Fig. 7b. Figure 7b further shows that all clouds observed at BBM overlap with the three families of clouds detected at Niamey (grey crosses) (21 clouds in cluster 1, 45 in cluster 2 and 28 in cluster 3), even if their bases are slightly higher. The histograms of Fig. 6 are split according to the contribution of each of these three clusters. Clusters 2 and 3 are largely differentiated by their cloud bases; cluster 2 has high bases (between 5160 m and 7650 m), while cluster 3 has low bases (between 2580 m and 5400 m). Cluster 1 has bases between 2550 m and 7400 m. Cluster 1 mainly differs from clusters 2 and 3 by the larger thickness of its clouds: it is greater than 640 m and reaches up to 4220 m. Most clusters 2 and 3 clouds have thicknesses less than 500 m (between 67 m and 725 m (cluster 2) and between 20 m and 1285 m (cluster 3)). Consistently, clouds from cluster 1 also have higher reflectivities

(between -32 dBZ and -4 dBZ) than those of clusters 2 and 3 (between -34 dBZ and -20 dBZ and between -40 dBZ and -13 dBZ for clusters 2 and 3 respectively). These clouds therefore contain the largest water contents. They are also the only clouds that predominantly precipitate with 64% of precipitating clouds whereas clusters 2 and 3 include 6% and 14% precipitating clouds respectively (not shown). Note that clouds in clusters 2 and 3 are of “shorter duration”: they last on average an hour and a half (86% with less than 3 hours) whereas in cluster 1, the "duration" is on average seven and a half hours (not shown). In summary, clouds in clusters 2 and 3 differ from clouds in cluster 1 by their macrophysical properties (notably thickness and "duration") but also by their microphysical properties (in particular reflectivity and precipitation).

For illustration, three clouds belonging to two different clusters are shown in Fig. 1b. The two thicker clouds which have a large intra-cloud reflectivity variance belong to cluster 1. The other cloud is thin, it has a low intra-cloud reflectivity variance; it belongs to cluster 3 (see Fig. 1b).

As discussed earlier, there are more mid-level clouds during the monsoon. There is therefore an increase of the cloud number in the clusters during this period, in particular in cluster 3 whose frequency of occurrence is the highest from July until October (Fig. 8). This cluster decreases later than the others; it is the only cluster with clouds in November. Possessing low bases, it persists in the season thanks to the humidity present in the lower layers. Cluster 2 also displays a seasonal cycle but of reduced amplitude and with an earlier increase (June) compared to cluster 3. Clouds belonging to this cluster are also present at the beginning of the year. Finally, cluster 1 has the weakest seasonal cycle, with an earlier increase in May. Outside the monsoon season, clouds of cluster 1 can be associated with the TP events since they generate long lasting and partly precipitating mid-level clouds (Fröhlich et al., 2013; Knippertz and Fink, 2009).

On this basis of macro- and microphysical characteristics observed on these three clusters, by analogy we can already establish resemblances with the clouds defined by McFarlane *et al.* (2013) who also defined these clouds in the tropical western Pacific Ocean region: congestus with cloud base lower than 4 km, cloud top between 4 and 8 km and cloud thickness higher than 1.5 km,

altocumulus with cloud base between 4 and 8 km, cloud top between 4 and 8 km and cloud thickness lower than 1.5 km and altostratus with cloud base between 4 and 8 km, cloud top between 4 and 8 km and cloud thickness higher than 1.5 km. This coincides with the criteria observed except for the cloud thickness criteria of altostratus.

4.3. Thermodynamics of mid-level clouds

We now analyse if these different families of mid-level clouds also indicate different thermodynamic regimes. Several mean thermodynamic characteristics obtained from radiosondes for the three clusters before, during and after (as defined in section 3.4) the cloud occurrence are shown in Fig. 9, where the origin of the vertical axis is the cloud base. The mean cloud base is used for this aim and not the cloud base height at the sampling time, keeping in mind that at these heights the radar-lidar profiles may not be perfectly collocated with the sounding profiles. The underlying assumption is then that the thermodynamical profile provides an indication of the characteristic of the environment of a cloud, including its averaged macrophysical properties. For each cluster, the anomalies were computed as the difference between the average for a given period (i.e.; before/during/after a cloud occurrence) and the average of all the soundings over all periods. Most often, a negative potential temperature anomaly and a positive specific humidity anomaly are observed during cloud occurrence, except for cluster 1, with maximum anomalies at the cloud top (not shown). For clusters 2 and 3, the profiles before and after the cloud occurrence are close, i.e. we observe a quick recovery. By contrast, for cluster 1, there is a departure of the profiles after the cloud occurrence with a cooling of about 1K and a moistening of about 1g.kg^{-1}. This suggests a significant transport of water vapour by these clouds. The relative humidity also increases during the cloud occurrence in the cloudy layer (mainly at cloud base) and decreases rapidly below the cloud base and above the cloud top, notably for the clusters 2 and 3. Heymsfield *et al.* (1990) also observed the same structure for an altocumulus cloud during an aircraft campaign at the end of

October in Wisconsin. Moreover, they observed low cloud ice concentrations as in Niamey. Another case study conducted by Schmidt *et al.* (2014) in August 2010 in Florida also focused on an altocumulus. As for Niamey clouds, this cloud, with a thickness smaller than 300 m, had a mixed-phase composition with very low quantities of supercooled liquid droplets. Ansmann *et al.* (2009) noticed the same feature in geometrically and optically thin altocumulus over the tropical North Atlantic. Their cloud tops were almost all composed of liquid and their cloud bases of ice. Ice could be formed by polluted air consisting of biomass-burning smoke and Saharan dust aerosol (DeMott *et al.*, 2003, 2009). According to Ansmann *et al.* (2009), another characteristic of these clouds is their capacity to form by evaporation or sublimation of precipitation in deep virga layers below cloud base. However, in our case, clouds of cluster 2 do not precipitate and very few possess virga (only 2 clouds). Clouds with virga are more frequent in cluster 1, which could perhaps be further divided into two clusters: those associated with convection and those associated with altocumulus possessing virga. During the cloud occurrence, the cluster 2 is in warmer and less humid environment than clusters 1 and 3. For this last cluster, a thick zone of higher specific humidity is observed below cloud base (Fig. 9k), this suggests that these clouds are fed with water vapour from the lower layers.

Johnson *et al.* (1999) and Riihimaki *et al.* (2012) argued that mid-level clouds could be formed by detrainment. According to Bretherton and Smolarkiewicz (1989), a stable environment would control detrainment. Thus, we investigated whether enhanced stability is found in the cloud environment by determining the inversions in the sounding profiles. Firstly, we observed with Niamey soundings that inversions are frequently found around the level of mid-level cloud occurrence (not shown). The inversion height increases during the monsoon period and decreases in autumn. Of the 482 mid-level clouds observed at Niamey, the thermodynamical environment of 233 clouds was sampled with at least one radiosonde, among which 216 are characterized by at least one inversion.

We then distinguished situations where the inversion height is located above the cloud top

and those where the inversion height is below cloud top (even if close). Inversions are preferentially located above the cloud top in particular for clusters 2 and 3 (see dashed part of the vertical bars in Fig. 10). Note also that inversions associated with those clusters are stronger than inversions associated with cluster 1. This points to a possible role of the inversion in blocking the cloud vertical development, in a similar way as proposed by Johnson *et al.* (1996) and Zuidema (1998). For cluster 1, inversions are weak and mainly located below cloud tops, which suggests that those clouds have sufficient buoyancy to overcome this enhanced stability layer. However for Riley and Mapes (2009), at these altitudes, a stable environment and cloud occurrence are not necessarily paired. According to them, a stable layer created at the cloud top by radiative cooling can not explain the detrainment phenomenon and consequently the formation of mid-level clouds. Here, detrainment refers to a mesoscale lateral spreading of hydrometeors/water vapour at a capping inversion and this is an especially relevant process for clouds of clusters 2 and 3.

4.4. Radiative impacts of mid-level clouds

The effect of mid-level clouds on the surface radiative fluxes depends on many factors including cloud properties, surface properties, solar elevation angle, hours of the day and seasons (Zhang *et al.*, 1996). The three mid-level cloud clusters are characterized by differences in macrophysical and microphysical properties as well as by different occurrences during the year. Here we analyse whether these clusters are also characterized by distinct radiative effects. Figure 11 quantifies the monthly-mean mid-level cloud radiative forcing in the shortwave (SW) (a) and in the longwave (LW) (b) domains estimated from the 15-minute sampled data. These results also extend the study of Bouniol *et al.* (2012) to the entire year. Table 2 shows for each cluster: i/ the Cloud Radiative Effects (CRE) SW flux over the clear-sky (CS) SW flux at the surface for mid-level clouds (MLC):

$$\text{BOA\_SW}_n = \frac{SW\downarrow_{MLC} - SW\downarrow_{CS}}{SW\downarrow_{CS}} \quad \text{(i)}$$

ii/ the upwelling shortwave radiation at the top of atmosphere ($SW\uparrow_{MLC}$) over the clear-sky SW flux:

$$\text{TOA\_SW}_n = \frac{SW\uparrow_{MLC}}{SW\downarrow_{CS}} \quad \text{(ii)}$$

iii/ the CRE LW flux:

$$\text{BOA\_LW} = LW\downarrow_{MLC} - LW\downarrow_{CS} \quad \text{(iii)}$$

iv/ the upwelling longwave radiation at the top of atmosphere ($LW\uparrow_{MLC}$):

$$\text{TOA\_LW} = LW\uparrow_{MLC} \quad \text{(iv)}$$

The normalization by the clear-sky SW flux removes the dependence on solar elevation angle. In the longwave domain, the measures are much less sensitive to the diurnal cycle and they are not normalized by the clear-sky LW.

4.4.1. Shortwave domain

In Figure 11a, the monthly mean incoming shortwave radiative impact due to mid-level clouds at the surface, calculated from the difference between the composite of mid-level clouds and the composite of the observations in clear-sky for a given month between 0800 UTC and 1600 UTC, ranges between -220 and -20 $W.m^{-2}$. For January, February and March, the mean impact varies between -150 and -100 $W.m^{-2}$. The annual maximum is observed in April. During the monsoon, a maximal amplitude is observed in July and reach the mean value of -180 $W.m^{-2}$ linked to the progression of the monsoon flux over the continent (Bouniol *et al.*, 2012) while for the other months the mean impact is around -100 $W.m^{-2}$. In October, the mean impact decreases to around -50 $W.m^{-2}$ and then becomes close to zero in November. These results are close to those obtained by Bouniol *et al.* (2012).

The BOA_SW_n reveals that cluster 1 clouds (the thickest, with high reflectivities) have the

strongest SW impact at the surface (it is three times stronger than for the clouds of clusters 2 and 3). Cluster 1 clouds have also the strongest impact for each month except in May (not shown). However, the cloud sample is not large enough to get robust conclusions about the seasonal evolution of the SW radiative effect for the different clusters. The TOA_SW_n reveals that at the top of atmosphere (TOA), there are less disparities between clusters even if cluster 1 slightly dominates again. In summary, clouds of cluster 1, which are probably optically thicker (higher reflectivity as well as deeper clouds), may absorb more of the incoming shortwave radiation (Chen *et al.*, 2000). We observe a higher SW CRE for cluster 1 than cluster 3, and for cluster 3 than cluster 2.

4.4.2. Longwave domain

Figure 11b shows the monthly mean incoming longwave radiation due to mid-level clouds, calculated from the difference between the composite of mid-level clouds and the composite of the observations in clear-sky for a given month. The mean longwave CRE at the surface, which measures the greenhouse effect of clouds on the surface energy balance, fluctuates between 10 and 60 $W.m^{-2}$. These impacts are greater during the dryer months (January, February, April, October and November), and decrease during the monsoon (down to less than 20 $W.m^{-2}$), when the water vapour amount is maximum and damp the radiative impact of mid-level clouds. In other words, during the monsoon, there is a strong greenhouse effect of water vapour, and this tends to reduce the impact of clouds in the longwave domain. Stephens *et al.* (2012) also observed a systematic decrease of LW CRE at the surface above a given precipitable water threshold.

The distribution of these impacts by clusters indicates that cluster 1 has more impacts and especially during the winter months compared to clusters 2 and 3 (not shown). During the monsoon, it had slightly more impact in June and September than the other two clusters. On average, the longwave impact is 26 $W.m^{-2}$ (25^{th} percentile: 7.7 $W.m^{-2}$ and 75^{th} percentile: 41.7 $W.m^{-2}$) which is consistent with cloud radiative impacts derived for mid-level clouds in the tropical western Pacific

Ocean region (McFarlane *et al.*, 2013 and Burleysson *et al.*, 2015). During the monsoon period, clouds in cluster 3 have more radiative impact than clouds in cluster 2. This is also observed in the annual average: cluster 3 clouds have a LW CRE of 20 $W.m^{-2}$ (25^{th} percentile: 7.3 $W.m^{-2}$ and 75^{th} percentile: 29.1 $W.m^{-2}$) whereas cluster 2 clouds have a LW CRE of 19 $W.m^{-2}$ (25^{th} percentile: 3.8 $W.m^{-2}$ and 75^{th} percentile: 27.6 $W.m^{-2}$) (in the literature 19 $W.m^{-2}$ and 16 $W.m^{-2}$ respectively; McFarlane *et al.*, 2013; Burleyson *et al.*, 2015). At the top of atmosphere, the TOA_LW reveals that the clusters 2 and 3 clouds have more radiative impact than clouds in cluster 1. However, few cloud objects have allowed to obtain these mean values, due to multi-layer scenes and few clear-sky scenes, leading to large spreads.

Overall, we observed that mid-level clouds at the surface have a cooling effect of -18 $W.m^{-2}$ (combining shortwave and longwave effects). At the TOA, in the Tropics, Bourgeois et al. (2016) found a net average radiative effect of mid-level clouds of -0.6 $W.m^{-2}$ with -2.4 $W.m^{-2}$ and 1.8 $W.m^{-2}$ in the SW and LW domains respectively. However, during the monsoon period, they observed a warming effect in the Saharan region which varies between -0.2 and 1.0 $W.m^{-2}$. In the Tropics, the net radiative effect of all clouds is about - 20 $W.m^{-2}$ in HadGAM1 climate model and CERES data (Su et al., 2010). At the ARM Southern Great Plains site, in the midlatitude, Mace et al. (2006) found that mid-level clouds have a slightly cooling effect at the TOA and a heating effect at the surface.

5. Conclusion

To document the macro- and microphysical characteristics of mid-level clouds, located around 6 km height, the atmospheric environment within which they occur as well as their radiative properties in West Africa, we combined three datasets including active sensors: two from ground-based stations deployed respectively at the Sahelian site of Niamey in 2006 and at the Saharan site

of Bordj Badji Mokhtar in June 2011 and one obtained from CloudSat-CALIPSO satellites.

The mid-level clouds in this region are present throughout the year with a larger frequency of occurrence during the monsoon (June to September). They also predominantly occur in the early morning. The satellite data provided a broader regional view. They showed the increased presence of mid-level clouds in the more humid southern and western parts of West Africa. However, an enhancement of mid-level clouds over the Sahara during the monsoon is also observed, possibly related to the SHL dynamics, and consistent with an increased occurrence of a deep boundary layer over the Sahara allowing clouds to form, as well as detrainment from deep convection over the Sahara and in the South over the Sahel. We found that over West Africa, mid-level clouds are predominantly thin and mainly composed of liquid water.

Three different cloud types have been identified at Niamey, using a clustering method: one with low cloud bases (cluster 3), one with high cloud bases (cluster 2) and another with large cloud thicknesses (cluster 1). This study sought to highlight differences in macro- and microphysical properties, thermodynamics and radiative properties associated with these three clusters. We found dissimilarities in (i) reflectivity (clouds of cluster 1 have higher reflectivities than clouds of clusters 2 and 3, suggesting a higher water content in this cluster), (ii) variability of reflectivities (clouds of cluster 1 have a higher variability of reflectivities than clouds of clusters 2 and 3), (iii) composition (clouds of cluster 1 contain more ice in terms of volume fraction than clouds of clusters 2 and 3 which contain more liquid water in terms of volume fraction), and consequently (iv) precipitation (clouds of cluster 1 are generally precipitating with 64% of precipitating clouds whereas clouds of clusters 2 and 3 are mainly non-precipitating with 6% and 14% of precipitating clouds respectively). Few differences appear in the macro- and microphysical characteristics of clusters 2 and 3 clouds. Nevertheless, the annual cycles of these two clusters are distinct. Clouds of clusters 2 and 3 mainly occur "before" and "during" the monsoon and "during" and "after" the monsoon respectively, whereas clouds of cluster 1 mainly occur during the monsoon. Clouds of clusters 2 and 3 share some thermodynamics properties, e.g. their cloud tops are associated with sharp inversions,

which suggests a role of these inversions in limiting the vertical development of these clouds. By contrast, no such inversion is found for clouds of cluster 1. Moreover, some obvious co-fluctuations are found in the annual cycles of mid-level cloud frequency of occurrence, CAPE (Convection Available Potential Energy) and CIN (Convective Inhibition), in particular with cluster 1, with a higher frequency of occurrence during the monsoon when CAPE is higher and CIN lower (not shown). Finally, clouds of cluster 1 differentiate again from clouds of clusters 2 and 3 by their higher radiative impact in both shortwave and longwave domains.

Through these analyses, it seems plausible that clouds of cluster 1 are associated with convective processes (these clouds share similarities with the congestus defined by Johnson et al. (1999) and Zuidema (1998)). The moisture origin of the cluster 1 clouds would therefore come from the lower layers. However, the clouds of clusters 2 and 3 show properties closer to stratiform clouds (Ansmann *et al.*, 2009; Heymsfield *et al.*, 1990; Schmidt *et al.*, 2014), the moisture source in the mid-troposphere leading to such cloud is therefore more enigmatic. The use of back trajectories from cloud location as well as idealized simulations could help in a future study to determine the origin of the moisture as well as to better understand the mechanisms leading to condensation and formation of these clouds. We also plan to investigate the contribution of these clouds in the water and energy cycle in West Africa and to analyse their role in the West African monsoon as well as in the dynamics of the SHL.

These clouds are often poorly represented in numerical weather prediction models (Bodas-Salcedo et al., 2008) and climate models (Roehrig *et al.,* 2013). Indeed, this is a challenge to represent these very thin clouds and their mixed-phase characteristics. Furthermore, our study highlights that there is not a unique mid-level cloud type, and that different physical processes are at play in the occurrence of these different types (convective and stratiform origins). The database constructed in this study provides an excellent basis to evaluate the capacity of different models ranging from cloud resolving (Marsham *et al.*, 2006) to regional convection permitting (Pearson *et al.*, 2010; Lean *et al.*, 2008) up to climate (Roehrig *et al.*, 2013).

Acknowledgements

The Niamey AMF data were obtained from the Atmospheric Radiation Measurement (ARM) Program Archive of the Department of Energy. There are available on the Cloudnet website (the Cloudnet project was funded by the European Union from Grant EVK2-2000-00065). We also thank E. O'Connor at the University of Reading who performed the processing on Niamey AMF data. The Bordj Badji Mokhtar data were obtained from ICAS and NCAS of Leeds University during the Fennec campaign. CloudSat data are obtained from CIRA of Colorado State University. ICARE and NASA gave access to the CALIOP data. We would like to thank Florence Favot for technical assistance in computer science and Florent Beucher for helpful on tropical meteorology. The comments, and their diversity, of four anonymous reviewers have greatly improved this manuscript.

References

Ansmann A, Tesche M, Althausen D, Müller D, Seifert P, Freudenthaler V, Heese B, Wiegner M, Pisani G, Knippertz P, Dubovik O. 2008. Influence of Saharan dust on cloud glaciation in southern Morocco during the Saharan Mineral Dust Experiment. *J. Geophys. Res. Atmos.* **113:** D04210, DOI: 10.1029/2007JD008785.

Ansmann A, Tesche M, Seifert P, Althausen D, Engelmann R, Fruntke J, Wandinger U, Mattis I, Müller D. 2009. Evolution of the ice phase in tropical altocumulus: SAMUM lidar observations over Cape Verde. *J. Geophys. Res*. *Atmos.* **114:** D17208, DOI: 10.1029/2008JD011659.

Bodas-Salcedo A, Webb MJ, Brooks ME, Ringer MA, Williams KD, Milton SF, Wilson DR. 2008. Evaluating cloud systems in the Met Office global forecast model using simulated CloudSat radar reflectivities. *J. Geophys. Res. Atmospheres*, **113:** D00A13, DOI: 10.1029/2007JD009620

Bouniol D, Couvreux F, Kamsu-Tamo PH, Leplay M, Guichard F, Favot F, O'Connor EJ. 2012. Diurnal and seasonal cycles of cloud occurrences, types, and radiative impact over West Africa. *J. Appl. Meteorol. Climatol.* **51:** 534–553, DOI: 10.1175/JAMC-D-11-051.1.

Bourgeois Q, Ekman AML, Igel MR, Krejci R. 2016. Ubiquity and impact of thin mid-level clouds in the tropics. *Nat. Commun.* **7:** 12432, DOI: 10.1038/ncomms12432.

Bretherton CS, Smolarkiewicz PK. 1989. Gravity waves, compensating subsidence and detrainment around cumulus clouds. *J. Atmos. Sci.* **46:** 740–759.

Bühl J, Seifert P, Myagkov A, Ansmann A. 2016. Measuring ice- and liquid-water properties in

mixed-phase cloud layers at the Leipzig Cloudnet station. *Atmos. Chem. Phys.* **16:** 10609-10620, DOI: 10.5194/acp-16-10609-2016.

Burleyson CD, Long CN, Comstock JM. 2015. Quantifying diurnal cloud radiative effects by cloud type in the Tropical Western Pacific. *J. Appl. Meteorol. Climatol.* **54:** 1297–1312, DOI: 10.1175/JAMC-D-14-0288.1.

Chen T, Rossow WB, Zhang Y. 2000. Radiative effects of cloud-type variations. *J. Climate* **13:** 264–286.

Cuesta J, Edouart D, Mimouni M, Flamant PH, Loth C, Gibert F, Marnas F, Bouklila A, Kharef M, Ouchène B, Kadi M, Flamant C. 2008. Multiplatform observations of the seasonal evolution of the Saharan atmospheric boundary layer in Tamanrasset, Algeria, in the framework of the African Monsoon Multidisciplinary Analysis field campaign conducted in 2006. *J. Geophys. Res. Atmos.* **113:** D00C07, DOI: 10.1029/2007JD009417.

Cuesta J, Lavaysse C, Flamant C, Mimouni M, Knippertz P. 2010. Northward bursts of the West African monsoon leading to rainfall over the Hoggar Massif, Algeria. *Q. J. R. Meteorol. Soc.* **136:** 174–189, DOI: 10.1002/qj.439.

DeMott PJ, Sassen K, Poellet MR, Baumgardner D, Rogers DC, Brooks SD, Prenni AJ, Kreidenweis SM. 2003. African dust aerosols as atmospheric ice nuclei. *Geophys. Res. Lett.* **30**(**14**): 1732, DOI: 10.1029/2003GL017410.

DeMott PJ, Sassen K, Poellet MR, Baumgardner D, Rogers DC, Brooks SD, Prenni AJ, Kreidenweis SM. 2009. Corrections to ‘‘African dust aerosols as atmospheric ice nuclei’’. *Geophys.*

Res. Lett. **36:** L07808, DOI: 10.1029/2009GL037639.

Duvel JP. 1989. Convection over tropical Africa and the Atlantic Ocean during northern summer. Part I: Interannual and diurnal variations. *Mon. Wea. Rev.* **117:** 2782–2799.

Fröhlich L, Knippertz P, Fink AH, Hohberger E. 2013. An Objective Climatology of Tropical Plumes. *J. Climate* **26:** 5044-5060. DOI: 10.1175/JCLI-D-12-00351.1.

Garcia-Carreras L, Parker DJ, Marsham JH, Rosenberg PD, Brooks IM, Lock AP, Marenco F, Mcquaid JB, Hobby M. 2015. The turbulent structure and diurnal growth of the Saharan atmospheric boundary layer. *J. Atmos. Sci.* **72:** 693-713, DOI: 10.1175/JAS-D-13-0384.1

Gounou A, Guichard F, Couvreux F. 2012. Observations of diurnal cycles over a West African meridional transect: pre-monsoon and full-monsoon seasons. *Bound. Lay. Meteorol.* **144:** 329–357, DOI: 10.1007/s10546-012-9723-8.

Haikin N, Galanti E, Reisin TG, Mahrer Y, Alpert P. 2015. Inner structure of atmospheric inversion layers over Haifa Bay in the eastern Mediterranean. *Bound. Lay. Meteorol.* **156:** 471-487. DOI: 10.1007/s10546-015-0038-4.

Harries JE, Russell JE, Hanafin JA, Brindley H, Futyan J, Rufus J, Kellock S, Matthews G, Wrigley R, Last A, Mueller J, Mossavati R, Ashmall J, Sawyer E, Parker D, Caldwell M, Allan PM, Smith A, Bates MJ, Coan B, Stewart BC, Lepine DR, Cornwall LA, Corney DR, Ricketts MJ, Drummond D, Smart D, Cutler R, Dewitte S, Clerbeaux N, Gonzalez L, Ipe A, Bertrand C, Joukoff A, Crommelynck D, Nelms N, Llewellyn-Jones DT, Butcher G, Smith GL, Szewczyk ZP, Mlynczak PE, Slingo A, Allan RP, Ringer MA. 2005. The geostationary earth radiation budget project. *Bull.*

Am. Meteorol. Soc. **86**(7): 945−960.

Haynes JM, Stephens GL. 2007. Tropical oceanic cloudiness and the incidence of precipitation: Early results from CloudSat. *Geophys. Res. Lett.*, **34:** L09811, DOI: 10.1029/2007GL029335.

Heymsfield AJ, Miloshevich LM, Slingo A, Sassen K, O'C. Starr D. 1990. An observational and theoretical study of highly supercooled altocumulus. *J. Atmos. Sci.* **48:** 923-945.

Hoareau C, Keckhut P, Noel V, Chepfer H, Baray JL. 2013. A decadal cirrus clouds climatology from ground-based and spaceborne lidars above the south of France (43.9°N–5.7°E). *Atmos. Chem. Phys.* **13:** 6951–6963, DOI: 10.5194/acp-13-6951-2013.

Hogan RJ, O'Connor EJ. 2004. Facilitating cloud radar and lidar algorithms: The Cloudnet Instrument Synergy/Target Categorization product. Cloudnet documentation. [Available online at http://www.cloud-net.org/data/products/categorize.html. and at http://www.met.rdg.ac.uk/~swrhgnrj/publications/categorization.pdf]

Illingworth AJ, Hogan RJ, O'Connor EJ, Bouniol D, Brooks ME, Delanoë J, Donovan DP, Eastment JD, Gaussiat N, Goddard JWF, Haeffelin M, Klein Baltink H, Krasnov OA, Pelon J, Piriou JM, Protat A, Russchenberg HWJ, Seifert A, Tompkins AM, Van Zadelhoff GJ, Vinit F, Willén U, Wilson DR, Wrench CL. 2007. Cloudnet: Continuous evaluation of cloud profiles in seven operational models using ground-based observations. *Bull. Am. Meteorol. Soc.* **88:** 883–898. DOI: 10.1175/BAMS-88-6-883.

Jain AK, Dubes RC. 1988. Algorithms for Clustering Data. *Prentice-Hall, Englewood Cliffs.*

Jakob C, Tselioudis G. 2003. Objective identification of cloud regimes in the tropical western Pacific. *Geophys. Res. Lett.* **30:** 2082, DOI: 10.1029/2003GL018367.

Johnson RH, Ciesielski PE, Hart KA. 1996. Tropical inversions near the 0°C level. *J. Atmos. Sci.* **53:** 1838–1855.

Johnson RH, Rickenbach TM, Rutledge SA, Ciesielski PE, Schubert WH. 1999. Trimodal characteristics of tropical convection. *J. Climate* **12:** 2397–2418.

Kato S, Rose FG, Rutan DA, Charlock TP. 2008. Cloud effects on the meridional atmospheric energy budget estimated from Clouds and the Earth's Radiant Energy System (CERES) Data. *J. Climate* **21** (**17**)**:** 4223-4241, DOI: 10.1175/2008JCLI1982.1.

Knippertz P, Fink AH. 2009. Prediction of Dry-Season Precipitation in Tropical West Africa and Its Relation to Forcing from the Extratropics. *Weather and Forecasting* **24:** 1064–1084. DOI: 10.1175/2009WAF2222221.1.

Lavaysse C, Flamant C, Janicot S, Parker DJ, Lafore JP, Sultan B, Pelon J. 2009. Seasonal evolution of the West African heat low: A climatological perspective. *Clim. Dynam.* **33:** 3130330, DOI: 10.1007/s00382-009-0553-4.

Lean HW, Clark PA, Dixon M, Roberts NM, Fitch A, Forbes R, Halliwell C. 2008. Characteristics of high-resolution versions of the Met Office Unified Model for forecasting convection over the United Kingdom. *Mon. Wea. Rev.* **136:** 3408–3424.

Mace GG, Benson S, Kato S. 2006. Cloud radiative forcing at the Atmospheric Radiation

Measurement Program Climate Research Facility: 2. Vertical redistribution of radiant energy by clouds. *J. Geophys. Res.* **111:** D11S91, DOI:10.1029/2005JD005922.

MacQueen J. 1967. Some methods for classification and analysis of multivariate observations. *Western Management Science Institute* **233(75):** Task No. 047-041.

Marsham JH, Dobbie S, Hogan RJ. 2006. Evaluation of a large-eddy model simulation of a mixed-phase altocumulus cloud using microwave radiometer, lidar and Doppler radar data. *Q. J. R. Meteorol. Soc.* **132:** 1693-1715, DOI: 10.1256/qj.05.145.

Marsham JH, Hobby M, Allen CJT, Banks JR, Bart M, Brooks BJ, Washington R. 2013. Meteorology and dust in the central Sahara: Observations from Fennec supersite-1 during the June 2011 intensive observation period. *J. Geophys. Res. Atmos.* **118:** 4069–4089, DOI: 10.1002/jgrd.50211.

Marsham JH, Parker DJ, Todd MC, Banks JR, Brindley HE, Garcia-Carreras L, Roberts AJ, Ryder CL. 2016. The contrasting roles of water and dust in controlling daily variations in radiative heating of the summertime Saharan heat low. *Atmos. Chem. Phys.* **16:** 3563-3575, DOI: 10.5194/acp-16-3563-2016.

McFarlane SA, Long CN, Flaherty J. 2013. A climatology of surface cloud radiative effects at the ARM tropical western Pacific sites. *J. Appl. Meteorol. Climatol.* **52:** 996–1013, DOI: 10.1175/JAMC-D-12-0189.1.

Miller MA, Slingo A. 2007. The ARM Mobile Facility and its first international deployment: Measuring flux divergence in West Africa. *Bull. Am. Meteorol. Soc.* **88:** 1229–1244.

Pantillon F, Knippertz P, Marsham JH, Panitz HJ, Bischoff-Gauss I. 2016. Modeling haboob dust storms in large-scale weather and climate models. *J. Geophys. Res. Atmos*. **121:** 2090–2109, DOI: 10.1002/2015JD024349.

Parker DJ, Burton RR, Diongue-Niang A, Ellis RJ, Felton M, Taylor CM, Thorncroft CD, Bessemoulin P, Tompkins AM. 2005. The diurnal cycle of the West African monsoon circulation. *Q. J. R. Meteorol. Soc*. **131:** 2839–2860, DOI: 10.1256/qj.04.52.

Pearson KJ, Hogan RJ, Allan RP, Lister GMS, Holloway CE. 2010. Evaluation of the model representation of convective systems using satellite observations of outgoing longwave radiation. *J. Geophys. Res. Atmos.* **115:** D20206, DOI: 10.1029/2010JD014265.

Pope M, Jakob C, Reeder M. 2009a. Objective classification of tropical mesoscale convective systems. *J. Climate* **22:** 5797–5808, DOI: 10.1175/2009JCLI2777.1.

Protat A, Young SA, McFarlane SA, L'Ecuyer T, Mace GG, Comstock JM, Long CN, Berry E, Delanoë J. 2014. Reconciling Ground-Based and Space-Based Estimates of the Frequency of Occurrence and Radiative Effect of Clouds around Darwin, Australia. *J. Appl. Meteor. Clim*. **53:** 456-478.

Ramanathan V, Cess R, Harisson E, Minnis P, Barkstrom B, Ahmad A, Hartmann D. 1989. Cloud-radiative forcing and climate: Results from the Earth Radiation Budget Experiment. *Science* **243:** 57–63.

Redelsperger JL, Diedhiou A, Flamant C, Janicot S, Lafore JP, Lebel T, Polcher J, Bourlès B,

Caniaux G, De Rosnay P, Desbois M, Eymard L, Fontaine B, Geneau I, Ginoux K, Hoepffner M, Kane CSE, Law K, Mari C, Marticoréna B, Mougin E, Pelon J, Peugeot C, Protat A, Roux F, Sultan B, Van den Akker E. 2006. AMMA, un projet international et multidisciplinaire de la mousson ouest-africaine. *La Météorologie* **54:** 22–32.

Riihimaki LD, McFarlane SA, Comstock JM. 2012. Climatology and formation of tropical midlevel clouds at the Darwin ARM site. *Am. Meteorol. Soc.* **25:** 6835–6850, DOI: 10.1175/JCLI-D-11-00599.1.

Riley EM, Mapes BE. 2009. Unexpected peak near -15°C in CloudSat echo top climatology. *Geophys. Res. Lett.* **36:** L09819, DOI: 10.1029/2009GL037558.

Roehrig R, Bouniol D, Guichard F, Hourdin F, Redelsperger JL. 2013. The present and future of the West African monsoon: A process-oriented assessment of CMIP5 simulations along the AMMA transect. *Am. Meteorol. Soc.* **26:** 6471–6505, DOI: 10.1175/JCLI-D-12-00505.1.

Sassen K, Wang Z. 2008. Classifying clouds around the globe with the CloudSat radar: 1-year of results. *Geophys. Res. Lett.*, **35:** L04805, DOI: 10.1029/2007GL032591.

Sassen K, Wang Z. 2012. The clouds of the middle troposphere: composition, radiative impact, and global distribution. *Surv. Geophys.* **33:** 677–691, DOI: 10.1007/s10712-011-9163-x.

Schmidt JM, Flatau PJ, Yates RD. 2014. Convective cells in altocumulus observed with a high-resolution radar. *J. Atmos. Sci.* **71:** 2130–2154, DOI: 10.1175/JAS-D-13-0172.1.

Stein THM, Parker DJ, Delanoë J, Dixon NS, Hogan RJ, Knippertz P, Maidment RI, Marsham JH.

2011. The vertical cloud structure of the West African monsoon: A 4 year climatology using CloudSat and CALIPSO. *J. Geophys. Res.* **116:** D22205, DOI: 10.1029/2011JD016029.

Stephens GL, Vane DG, Boain RJ, Mace GG, Sassen K, Wang Z, Illingworth AJ, O'Connor EJ, Rossow WB, Durden SL, Miller SD, Austin RT, Benedetti A, Mitrescu C, CloudSat Science Team. 2002. The CloudSat mission and the A-Train: A new dimension of space-based observations of clouds and precipitation. *Bull. Am. Meteorol. Soc.* **83:** 1771–1790.

Stephens GL. 2005. Cloud feedbacks in the climate system: A critical review. *J. Climate* **18:** 237-273, DOI: 10.1175/JCLI-3243.1.

Stephens GL, Vane DG, Tanelli S, Im E, Durden S, Rokey M, Reinke D, Partain P, Mace GG, Austin R, L'Ecuyer T, Haynes T, Lebsock M, Suzuki K, Waliser D, Wu D, Kay J, Gettelman A, Wang Z, Marchand R. 2008. CloudSat mission: Performance and early science after the first year of operation. *J. Geophys. Res. Atmospheres.* **113:** D00A18, DOI: 10.1029/2008JD009982.

Stephens GL, Wild M, Stackhouse PW, L'Ecuyer T, Kato S, Henderson DS. 2012. The global character of the flux of downward longwave radiation. *J. Climate* **25:** 2329–2340, DOI: 10.1175/JCLI-D-11-00262.1.

Stokes GM, Schwartz SE. 1994. The Atmospheric Radiation Measurement (ARM) Program: Programmatic background and design of the cloud and radiation test bed. *Bull. Am. Meteorol. Soc.* **75:** 1201-1221.

Su W, Bodas-Salcedo A, Xu K-M, Charlock TP. 2010. Comparison of the tropical radiative flux and cloud radiative effect profiles in a climate model with Clouds and the Earth's Radiant Energy

System (CERES) data. *J. Geophys. Res.* **115:** D01105, DOI:10.1029/2009JD012490.

Tan I, Storelvmo T, Zelinka MD. 2016. Observational constraints on mixed-phase clouds imply higher climate sensitivity. *Science* **352:** 224–227.

Tompkins AM, Adebiyi AA. 2012. Using CloudSat cloud retrievals to differentiate satellite-derived rainfall products over West Africa. J. Hydrometeorol., **13:** 1810–1816, DOI: 10.1175/JHM-D-12-039.1.

Wang J, Rossow WB, Zhang Y. 2000. Cloud vertical structure and its variations from a 20-yr global rawinsonde dataset. *J. Clim.* **13:** 3041–3056.

Ward JH. 1963. Hierarchical Grouping to optimize an objective function. *J. Am. Statistical Association* **58:** Issue 301, 236-244.

Weaver CP. 2003. Efficiency of storm tracks an important climate parameter ? The role of cloud radiative forcing in poleward heat transport. *J. Geophys. Res.* **108(D1)**: 4018, DOI: 10.1029/2002JD002756.

Webster PJ, Lukas R. 1992. TOGA COARE: The Coupled Ocean-Atmosphere Response Experiment. *Bull. Am. Meteorol. Soc.* **73:** 1377–1416.

Winker D, Hunt W, McGill M. 2007. Initial performance assessment of CALIOP. *Geophys. Res. Lett.* **34:** L19803, DOI: 10.1029/2007GL030135.

Yasunaga K, Yoneyama K, Kubota H, Okamoto H, Shimizu A, Kumagai H, Katsumata M,

Sugimoto N, Matsui I. 2006. Melting layer cloud observed during R/V Mirai cruise MR01K05. *J. Atmos. Sci.* **63:** 3020-3032.

Zuidema P. 1998. The 600–800-mb minimum in tropical cloudiness observed during TOGA COARE. *J. Atmos. Sci.* **55:** 2220–2228.

Zhang MH, Lin WY, Klein SA, Bacmeister JT, Bony S, Cederwall RT, Del Genio AD, Hack JJ, Loeb NG, Lohmann U, Minnis P, Musat I, Pincus R, Stier P, Suarez MJ, Webb MJ, Wu JB, Xie SC, Yao MS, Zhang JH. 2005. Comparing clouds and their seasonal variations in 10 atmospheric general circulation models with satellite measurements. *J. Geophys. Res.* **110:** D15S02, DOI: 10.1029/2004JD005021.

Zhang T, Stammes K, Bowling SA. 1996. Impact of clouds on surface radiative fluxes and snowmelt in the Arctic and subarctic. *J. Climate* **9:** 2110–2123.

Zhang YC, Rossow W. 1997. Estimating meridional energy transports by the atmospheric and oceanic general circulations using boundary flux data. *J. Climate* **10:** 2358-2373, DOI: 10.1175/1520-0442(1997)010<2358:EMETBT>2.0.CO;2.

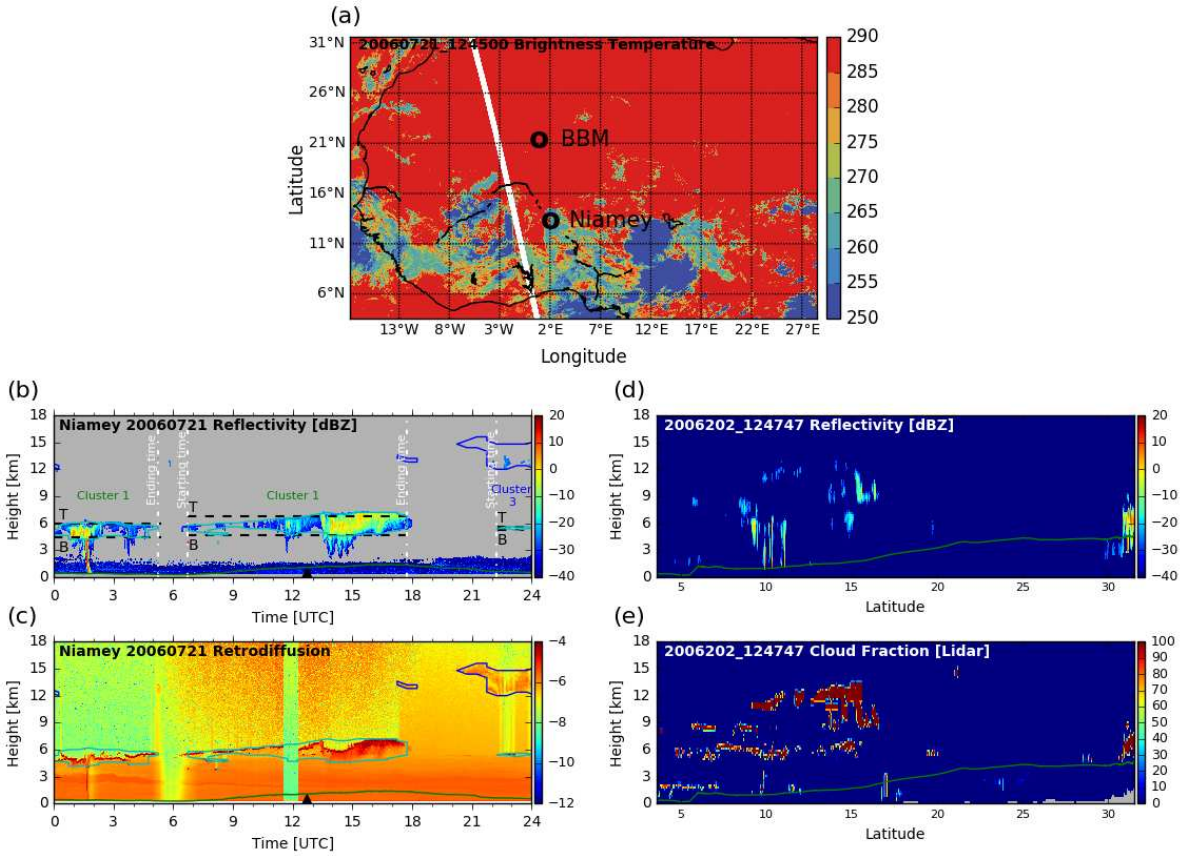

Figure 1. (a) Infrared (10.5 µm) SEVIRI brightness temperature (in K) on 21 July 2006 at 12:45. The CloudSat-CALIPSO track (shown in d) and e)) is overplotted in white. Niamey and BBM are indicated by black circles. (b-c) Time – height cross section of reflectivity (in dBZ) observed by the radar and log10 of attenuated backscattering coefficient at 532 nm (in sr^{-1} m^{-1}) observed by the lidar on the same day at Niamey (Niger). The lifting condensation level computed from the surface meteorology is overplotted in green. Cirrus and mid-level clouds are contoured in blue and cyan respectively. For each mid-level clouds, cloud base height (B), cloud top height (T), the starting and the ending times and their cluster affiliation are indicated. Black triangles indicate the starting time of the CloudSat-CALIPSO track. (d-e) Latitude – height cross section of reflectivity (in dBZ) observed by the CloudSat Cloud Profiling Radar and cloud fraction computed on the radar grid from the CALIPSO lidar on the same date from 12:47:47 between 3.575 - 31.575 °N. The lifting condensation level computed from the ECMWF-AUX is overplotted in green.

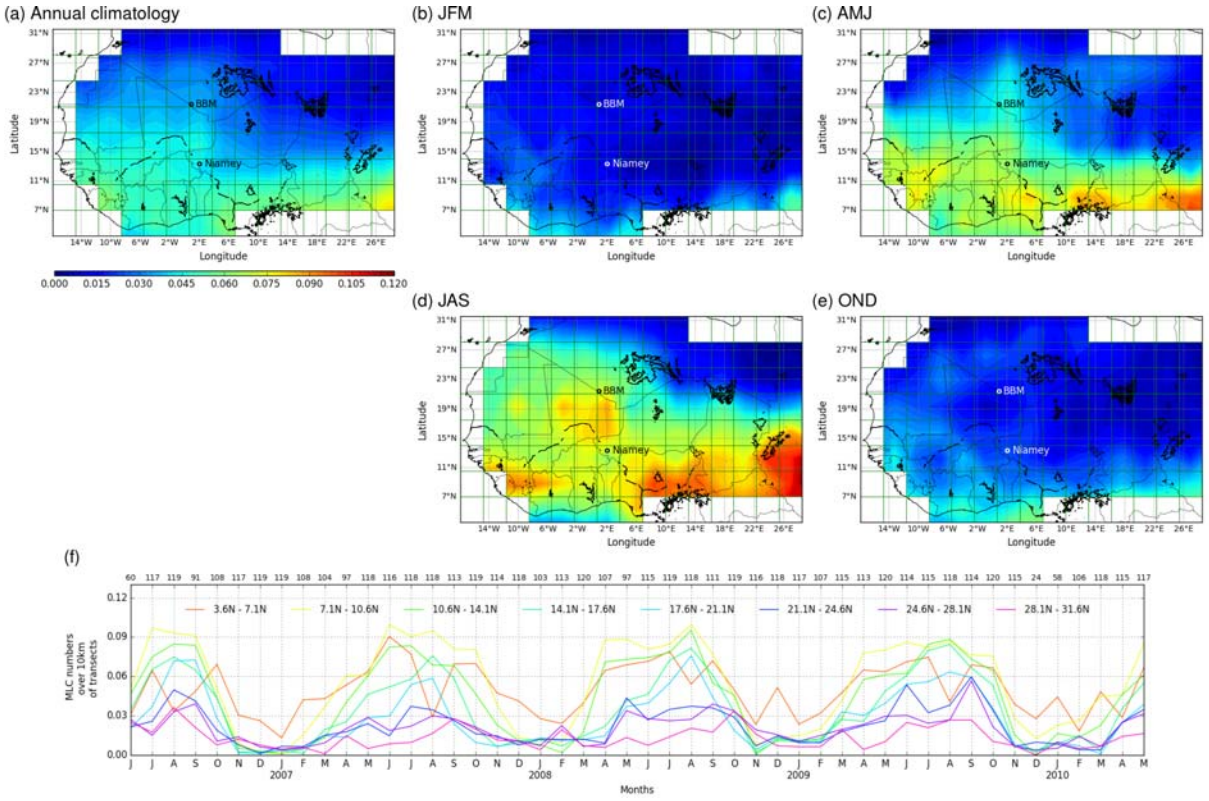

Figure 2. (a) Annual, (b) January-February-March (JFM), (c) April-May-June (AMJ), (d) July-August-September (JAS) and (e) October-November-December (OND) climatology of mid-level cloud density (number of clouds per kilometre of tracks) in km^{-1} from June 2006 to May 2010 in West Africa [3.575-31.575°N, 14.78°W-28.47°E] obtained with CloudSat-CALIPSO products. Here, these figures are computed from the cloud object identification. (f) Annual cycle of mid-level cloud density from June 2006 to May 2010 for latitudinal bands. The transect number for each month is reported at the top.

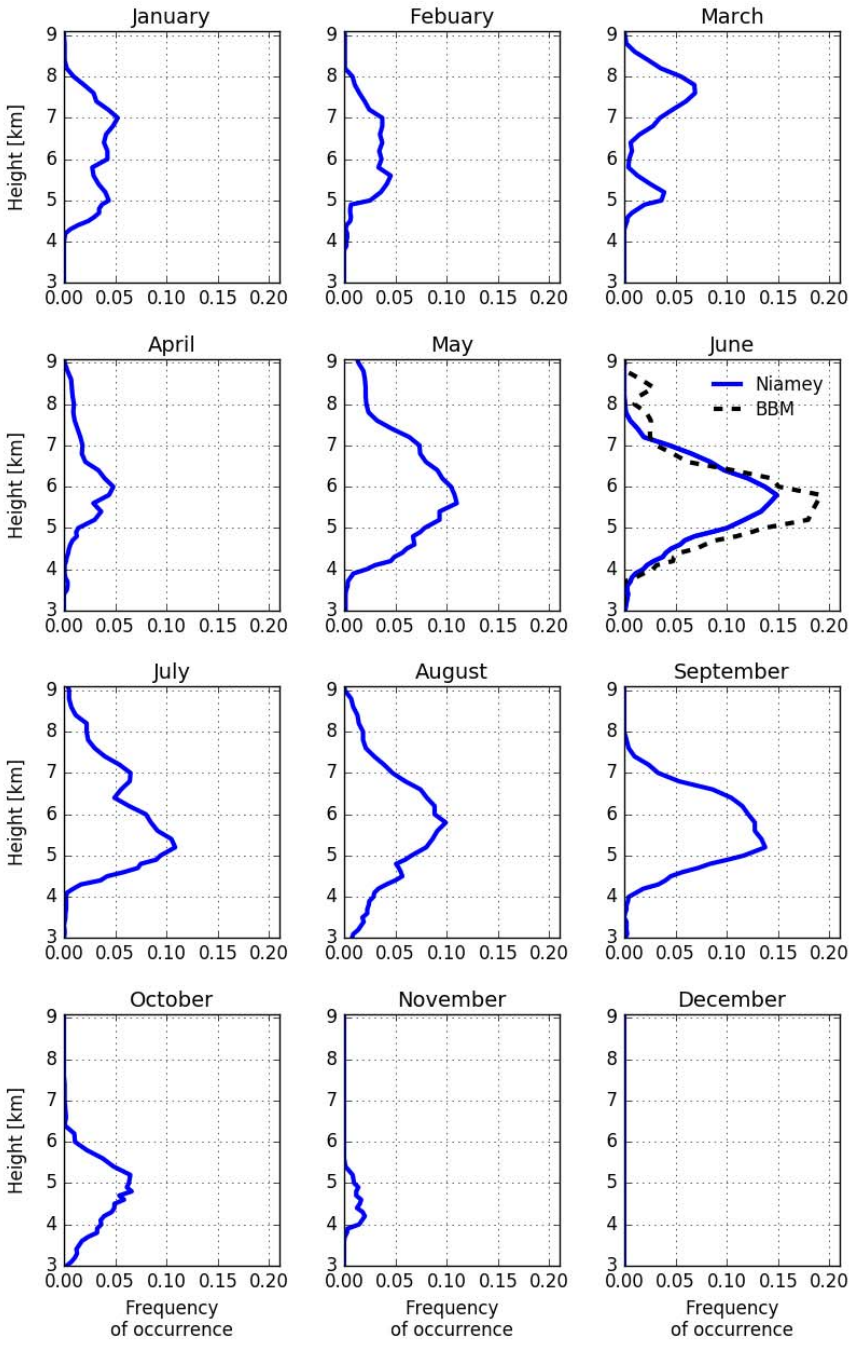

Figure 3. Annual evolution of monthly mid-level cloud frequency of occurrence (number of cloudy pixels over the total number of pixel observations at a given altitude with a 30 minute temporal resolution) at the ARM Mobile Facility at Niamey (Niger) in 2006 (blue) and at Bordj Badji Mokhtar (BBM) (Algeria) in June 2011 (black dotted line).

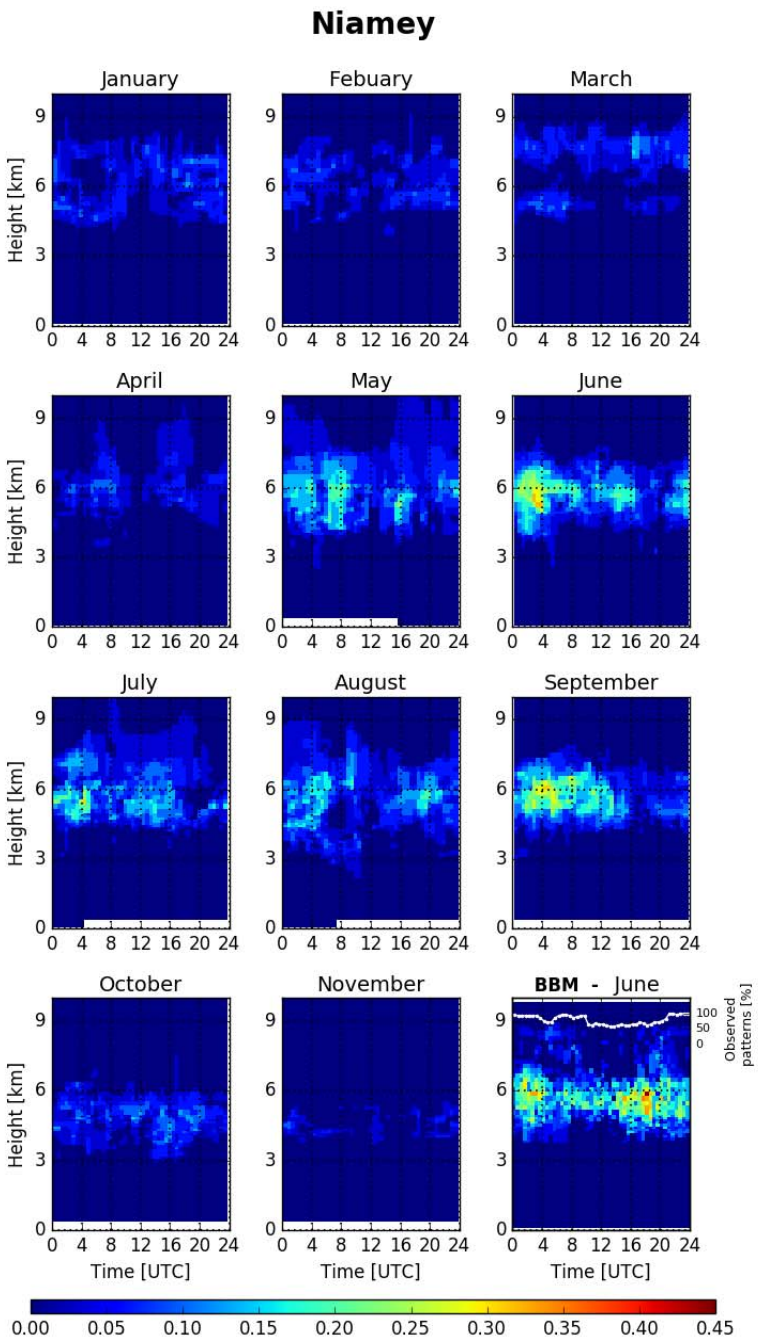

Figure 4. Annual evolution of the diurnal cycle of monthly mid-level cloud frequency of occurrence (for each 30 minutes range, number of cloudy pixels over the total number of pixel observations at a given altitude) at the ARM Mobile Facility at Niamey (Niger) in 2006 and (at bottom right) at Bordj Badji Mokhtar (BBM) (Algeria) in June 2011. This figure shows only

January to November months because no mid-level clouds were detected in December 2006 at Niamey.

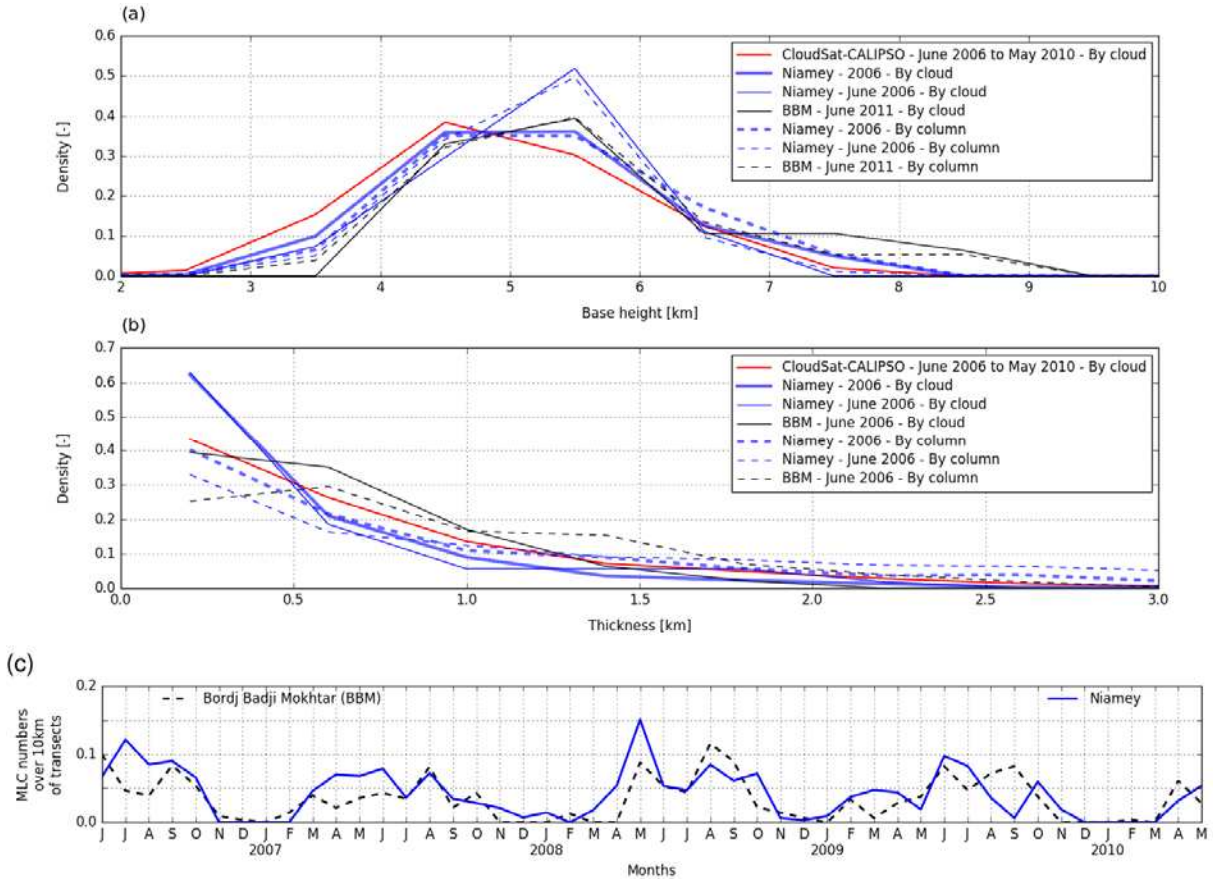

Figure 5. Distributions of (a) base height and (b) thickness detected by cloud (solid lines) and by column (dashed lines) observed at Niamey in 2006 (thick blue lines) and in June 2006 (thin blue lines), at BBM in June 2011 (thin black lines) and in the CloudSat-CALIPSO products (June 2006 to May 2010) for 3.575-31.575°N, 14.78°W-28.47°E (red lines). (c) Annual cycle of mid-level cloud density from June 2006 to May 2010 derived from the CloudSat-CALIPSO products for the elementary boxes where BBM [21.075-24.575°N, 0.668-3.758°E] (black dotted line) and Niamey [10.575-14.075°N, 0.668-3.758°E] (blue) are located.

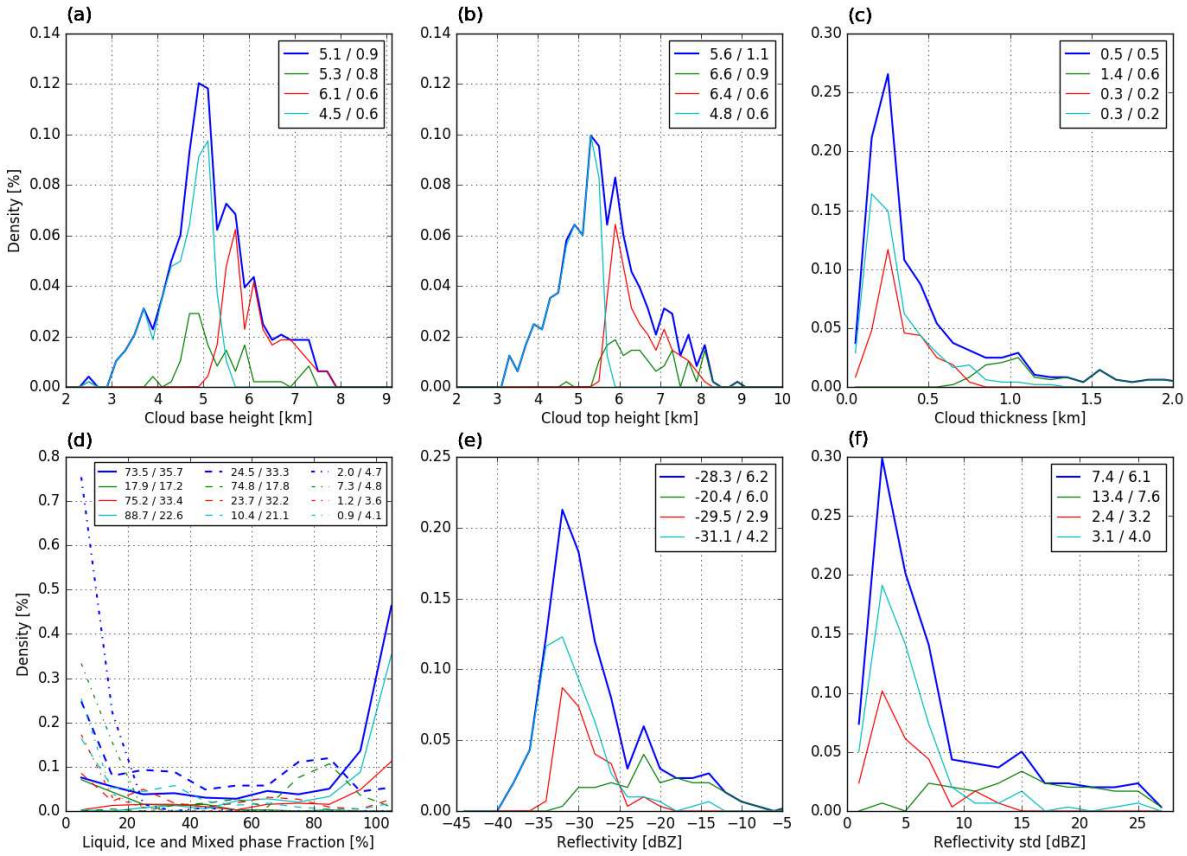

Figure 6. Distributions of (a) cloud base height, (b) cloud top height, (c) cloud thickness, (d) liquid (solid), ice (dashed) and mixed phase (dotted) fractions, (e) reflectivity, (f) standard deviation of reflectivity, for all cloud objects observed at Niamey in 2006 (i.e. 482 clouds) (blue lines) and for the three clusters obtained after the implementation of the HAC algorithm following the "Ward criterion". Cluster 1 is in green, cluster 2 in red and cluster 3 in cyan. For each distribution, the mean and the standard deviation of each characteristic for the 482 clouds and for each cluster are given in the top box.

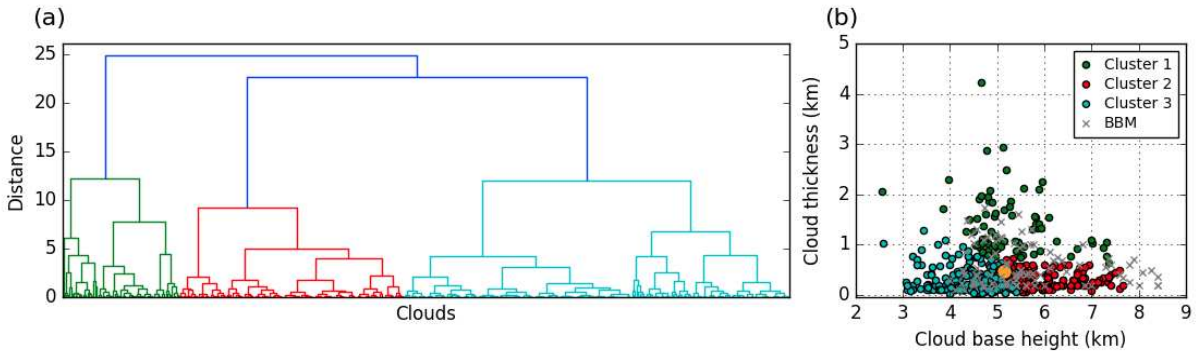

Figure 7. (a) Dendrogram associated with the HAC algorithm following the "Ward criterion". Cluster 1 is in green, cluster 2 in red and cluster 3 in cyan. (b) Cloud base height – cloud thickness distribution of the three clusters obtained after the implementation of the HAC algorithm with these two variables. Clusters, shown with colors, correspond to the three clusters of the figure (a). Each dot represents one of the 482 clouds observed in Niamey in 2006. The yellow dot represents the barycentre of all clouds. Clouds observed in BBM in June 2011 are represented by gray crosses.

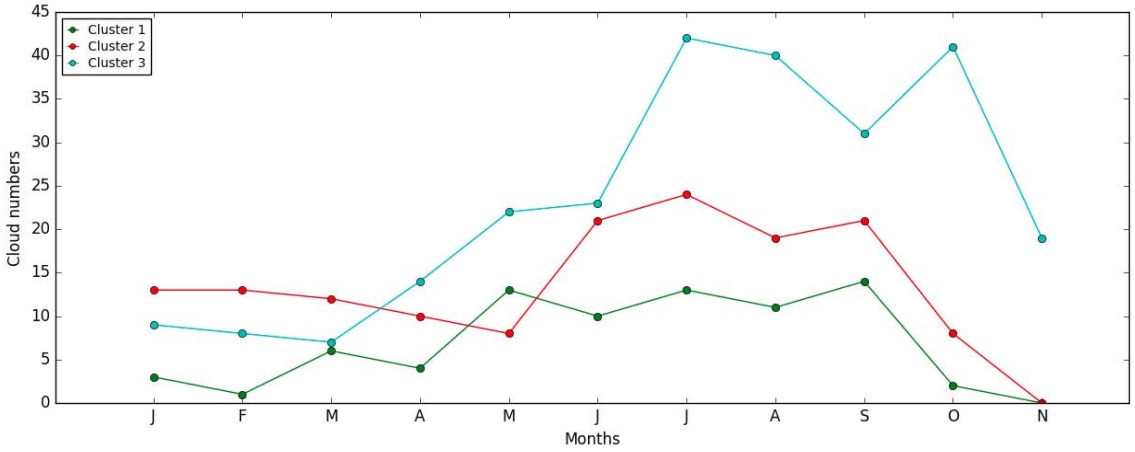

Figure 8. Monthly frequency of cloud numbers for each of the three clusters during the year 2006. The x-axis only extends from January to November as no mid-level clouds were detected in December 2006.

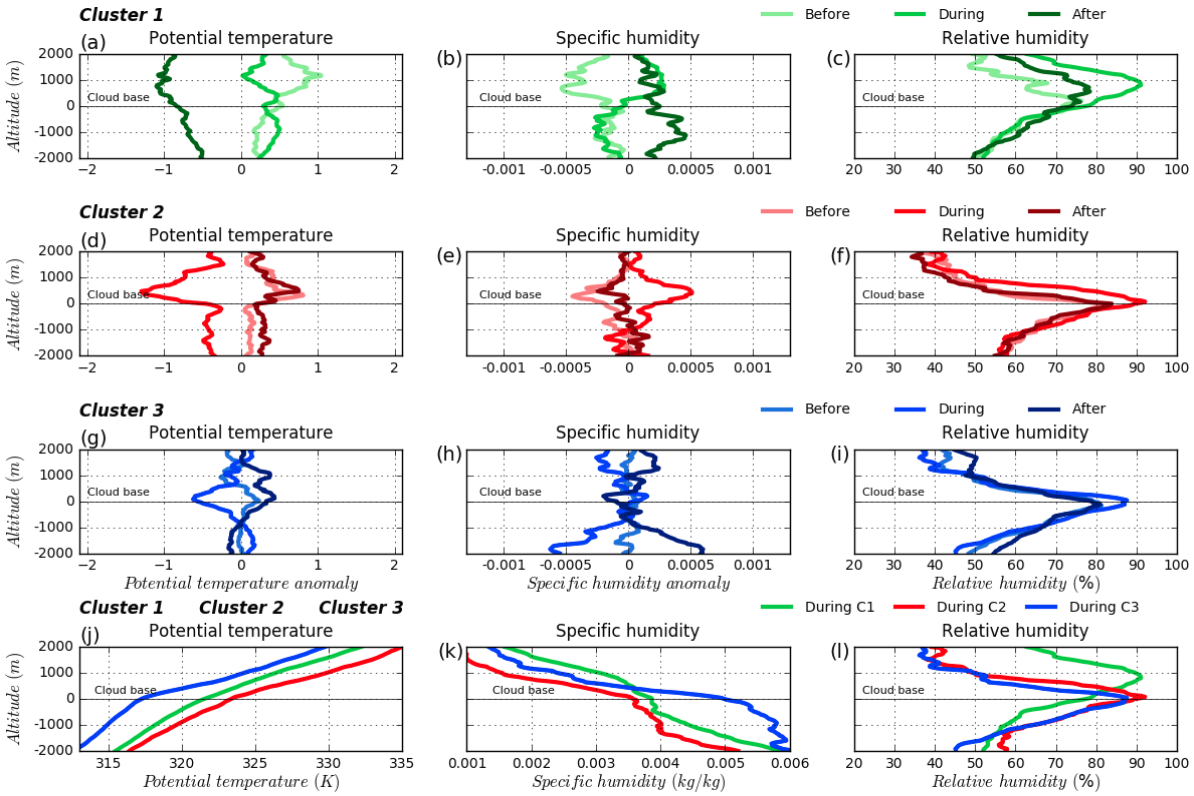

Figure 9. Vertical profile composites of thermodynamic characteristics with respect to the cloud bases and obtained from the Niamey radiosoundings: (a-d-g) potential temperature anomaly, (b-e-h) specific humidity anomaly and (c-f-i) relative humidity, before (light colors), during (normal colors) and after (dark colors) the cloud occurrence for each individual cluster (one line per cluster) and (j-k-l) in absolute values for the three clusters but only during the cloud occurrence.

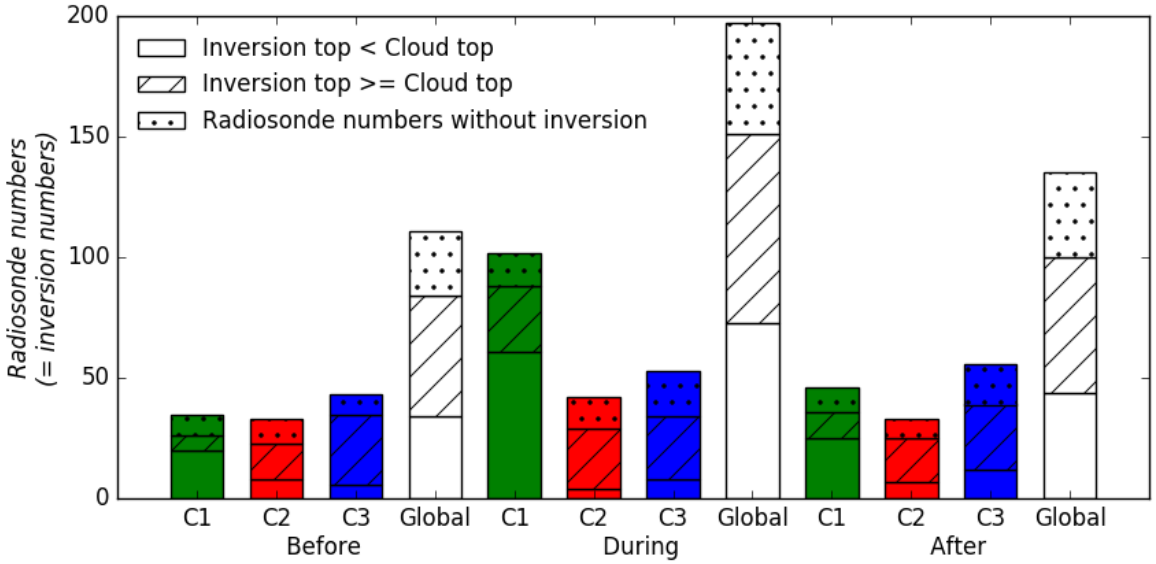

Figure 10. Histogram of the radiosonde numbers when the inversion top height is below the cloud top height (no pattern), when the inversion top height is above the cloud top height (hatched) and when no inversion is present (dotted) for each cluster (C1, C2 and C3) and for all of the clouds (Global), and each period (before, during and after the cloud occurrence).

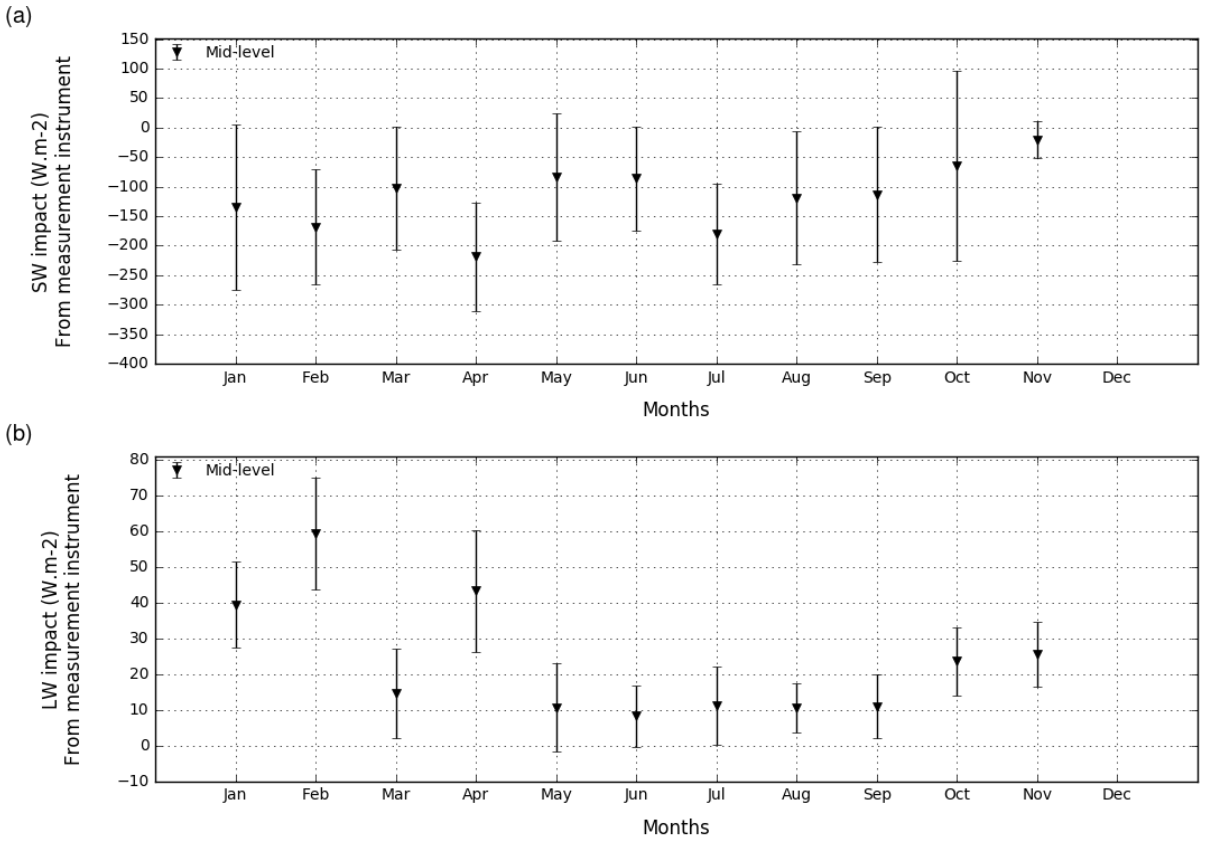

Figure 11. Surface mid-level cloud radiative effect at Niamey (a) in the shortwave and (b) in the longwave domains. Triangle symbols represent a monthly mean value and the vertical line twice the standard deviation.

Instruments	Measured parameters	Computed parameters	Spatial and temporal resolutions	Deployment duration
AMMA (ARM-Mobile Facility Niamey) - 2006				
Cloud radar (WACR) (95-GHz)	Reflectivity (Z) Doppler velocity Depolarisation ratio	Cloud occurrence (cf. section 4.2) and cloud classification and cloud masks and macro and microphysics properties (cf. section 4.3)	30 s / 40 m	1 April - 31 December 2006
Micropulse lidar (523 nm wavelength)	Backscattering coefficient (β) Depolarisation ratio	Cloud occurrence (cf. section 4.2) and cloud classification and cloud masks and macrophysics properties (cf. section 4.3)	30 – 60 s / 30 m	1 January - 31 December 2006
Radiosondes (RS92 GPS / Vaisala)	θ, T, q, p	Thermodynamics properties and inversions (cf. section 4.4)	6 hourly	1 January - 31 December 2006
Microwave Radiometer (MWR)		Cloud classification (cf. section 4.2)	20 s	1 January - 31 December 2006
Microwave Radiometer Profiler (MWR-P)		Cloud classification (cf. section 4.2)	5 min	1 January - 31 December 2006
Rain gauge		Cloud classification (cf. section 4.2)		1 January - 31 December 2006
Downwelling radiation (SKYRAD)	SW, LW	Radiation (cf. section 4.5)	1 min	1 January - 31 December 2006
Surface meteorology		Lifting condensation level	1 min	1 January - 31 December 2006
Fennec (Bordj Badji Mokhtar) - June 2011				
Doppler lidar (1550 nm wavelength)	Backscattering coefficient (β)	Cloud occurrence (cf. section 4.2) and cloud classification and cloud masks and macrophysics properties (cf. section 4.3)	30 s / 30 m	2 June - 1 July 2011
A-Train - CloudSat-CALIPSO - June 2006 to May 2010				
Cloud Profiling Radar (CPR) (94-GHz)	Reflectivity (Z)	Cloud occurrence (cf. section 4.2) and cloud classification and cloud masks and macro and microphysics properties (cf.	Cross-track : 1.4 km Along-track : 3.5 km / 480 m	June 2006 – May 2010

		section 4.3)		
Cloud-Aerosol Lidar with Orthogonal Polarization (CALIOP) (532 and 1064 nm wavelength)	Backscattering coefficient (β)	Cloud occurrence (cf. section 4.2) and cloud classification and cloud masks and macrophysics properties (cf. section 4.3)	333 m / 30 m - 60m	June 2006 – May 2010
MSG-1 - 2006				
Radiometer (GERB)	SW, LW	Radiation (cf. section 4.5)	15 min	1 January - 31 December 2006

Table 1. List of the different instruments with their time and space resolution, their deployment period, the measured and computed parameters. Note that this table is not an exhaustive list of instruments at the ground-based sites nor on the spaceborne plateform. Other parameters may be measured by the instruments, but not listed because not used in this study.

Ratios		Global	Cluster 1	Cluster 2	Cluster 3
BOA_SW_n (-)	Mean	-0.12	**-0.24**	-0.06	-0.07
	25^{th} percentile	-0.21	-0.36	-0.15	-0.17
	75^{th} percentile	0.02	-0.09	0.05	0.04
TOA_SW_n (-)	Mean	0.52	**0.55**	0.48	0.53
	25^{th} percentile	0.39	0.40	0.37	0.40
	75^{th} percentile	0.57	0.57	0.57	0.54
BOA_LW ($W.m^{-2}$)	Mean	16.25	**19.39**	13.50	16.56
	25^{th} percentile	4.42	5.18	0.23	6.84
	75^{th} percentile	25.59	28.34	21.77	24.12
TOA_LW ($W.m^{-2}$)	Mean	253	248	**254**	**255**
	25^{th} percentile	230.69	230.05	231.97	230.88
	75^{th} percentile	279.14	274.05	278.41	285.21

Table 2. Four mean ratios for all mid-level clouds and each cluster in the shortwave and in the longwave domains at the surface and at the top of atmosphere at Niamey in 2006. The 25^{th} percentile and the 75^{th} percentile are mentioned to provide uncertainty estimates. Only few clouds have allowed to obtain these mean values, due to multi-layer scenes and few clear-sky scenes, leading to large spreads. Therefore, these values are just indicative.